Article

www.the-innovation.org

Temperature acclimation in hot-spring snakes and the convergence of cold response

Chaochao Yan,[1,7] Wei Wu,[1,2,7] Wenqi Dong,[3,7] Bicheng Zhu,[1] Jiang Chang,[4] Yunyun Lv,[1,5] Shilong Yang,[3] and Jia-Tang Li[1,2,6,*]

*Correspondence: lijt@cib.ac.cn

Received: June 4, 2022; Accepted: July 28, 2022; Published Online: August 1, 2022; https://doi.org/10.1016/j.xinn.2022.100295

© 2022 The Author(s). This is an open access article under the CC BY-NC-ND license (http://creativecommons.org/licenses/by-nc-nd/4.0/).

GRAPHICAL ABSTRACT

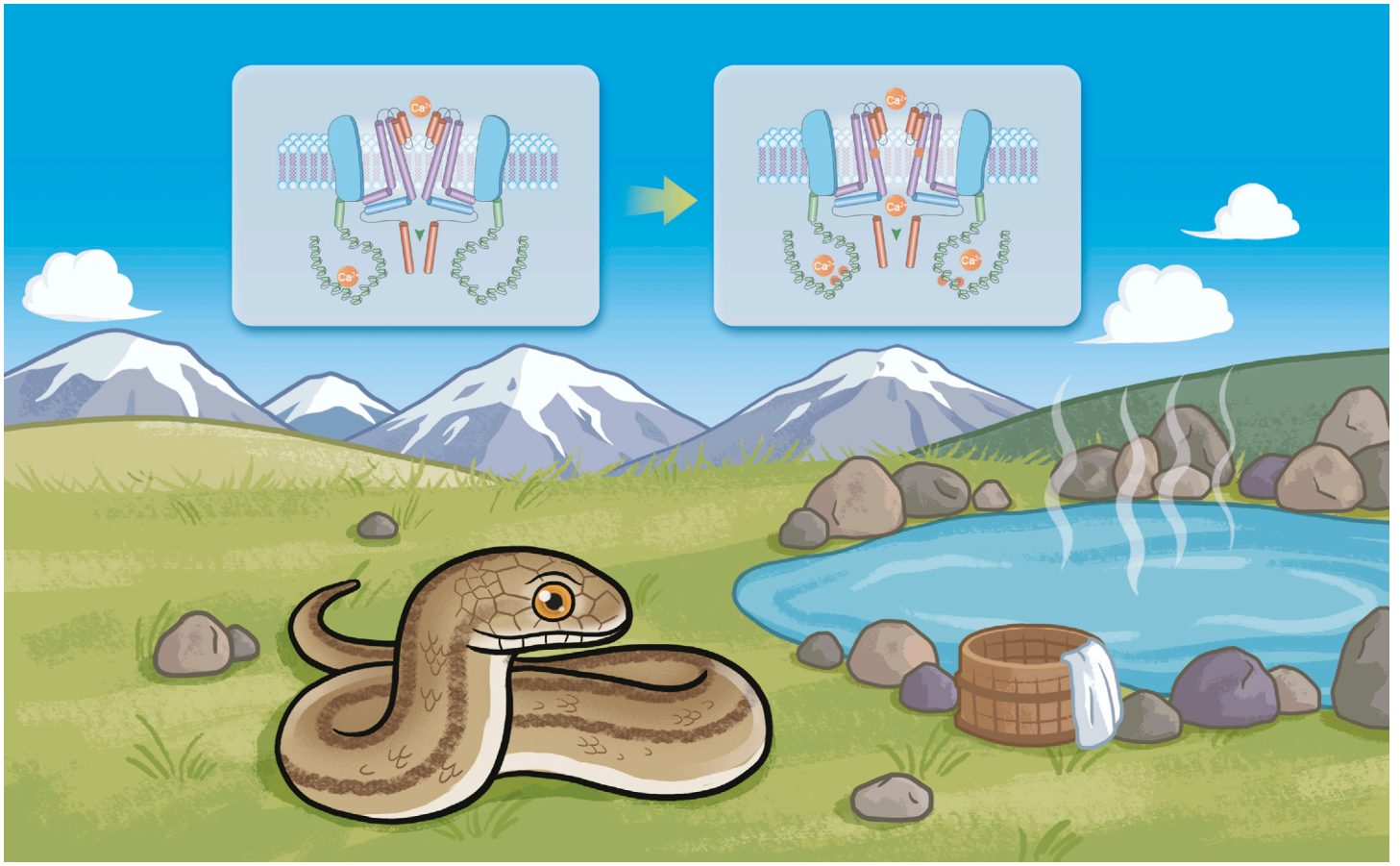

PUBLIC SUMMARY

- Hot-spring snakes prefer hot-spring habitats on the Qinghai-Tibet Plateau
- Genetic variation in the snakes contribute to the temperature acclimation
- Unique mutations in TRPA1 increase thermal sensitivity of the ion channel
- Different temperature-sensing strategies existed across snakes

Article

Temperature acclimation in hot-spring snakes and the convergence of cold response

Chaochao Yan,[1,7] Wei Wu,[1,2,7] Wenqi Dong,[3,7] Bicheng Zhu,[1] Jiang Chang,[4] Yunyun Lv,[1,5] Shilong Yang,[3] and Jia-Tang Li[1,2,6,*]

[1]CAS Key Laboratory of Mountain Ecological Restoration and Bioresource Utilization and Ecological Restoration and Biodiversity Conservation Key Laboratory of Sichuan Province, Chengdu Institute of Biology, Chinese Academy of Sciences, Chengdu 610041, China

[2]University of Chinese Academy of Sciences, Beijing 100049, China

[3]College of Wildlife and Protected Area, Northeast Forestry University, Harbin 660223, China

[4]State Key Laboratory of Environmental Criteria and Risk Assessment, Chinese Research Academy of Environmental Sciences, Beijing 100085, China

[5]College of Life Science, Neijiang Normal University, Neijiang, Sichuan 641100, China

[6]Center for Excellence in Animal Evolution and Genetics, Chinese Academy of Sciences, Kunming 650223, China

[7]These authors contributed equally

*Correspondence: lijt@cib.ac.cn

Received: June 4, 2022; Accepted: July 28, 2022; Published Online: August 1, 2022; https://doi.org/10.1016/j.xinn.2022.100295

© 2022 The Author(s). This is an open access article under the CC BY-NC-ND license (http://creativecommons.org/licenses/by-nc-nd/4.0/).

Citation: Yan C., Wu W., Dong W., et al., (2022). Temperature acclimation in hot-spring snakes and the convergence of cold response. The Innovation **3(5)**, 100295.

Animals have evolved sophisticated temperature-sensing systems and mechanisms to detect and respond to ambient temperature changes. As a relict species endemic to the Qinghai-Tibet Plateau, hot-spring snake (*Thermophis baileyi*) survived the dramatic changes in climate that occurred during plateau uplift and ice ages, providing an excellent opportunity to explore the evolution of temperature sensation in ectotherms. Based on distributional information and behavioral experiments, we found that *T. baileyi* prefer hot-spring habitats and respond more quickly to warmth than other two snakes, suggesting that *T. baileyi* may evolve an efficient thermal-sensing system. Using high-quality chromosome-level assembly and comparative genomic analysis, we identified cold acclimation genes experiencing convergent acceleration in high-altitude lineages. We also discovered significant evolutionary changes in thermosensation- and thermoregulation-related genes, including the transient receptor potential (TRP) channels. Among these genes, TRPA1 exhibited three species-specific amino acid replacements, which differed from those found in infrared imaging snakes, implying different temperature-sensing molecular strategies. Based on laser-heating experiments, the *T. baileyi*-specific mutations in *TRPA1* resulted in an increase in heat-induced opening probability and thermal sensitivity of the ion channels under the same degree of temperature stimulation, which may help the organism respond to temperature changes more quickly. These results provide insight into the genetic mechanisms underpinning the evolution of temperature-sensing strategies in ectotherms as well as genetic evidence of temperature acclimation in this group.

INTRODUCTION

Ambient temperature is one of the most critical environmental factors for organisms affecting many fundamental biological processes such as growth, survival, and reproduction. To adapt to the diverse range of thermal environments in the biosphere, animals have evolved a variety of behavioral, physiological, and molecular strategies for thermoregulation, resulting in a set of physiological and ecological traits appropriate to their habitat.[1] These thermoregulatory processes require sensitive thermal sensors, which are essential for detecting the spatiotemporal variation in environmental temperatures.[1–3] Therefore, evolutionary changes in thermosensory systems may improve thermal perception and responses, thereby facilitating animal survival and adaptation to the corresponding thermal niches.

The Qinghai-Tibet Plateau (QTP), also called the "Third Pole,"[4] contains unique biodiversity due to its remarkable orogenic history and significant glacial climate fluctuations.[5,6] In addition to strong ultraviolet (UV) radiation and relatively low oxygen partial pressure, organisms living on the plateau are exposed to low temperatures and extreme temperature fluctuations. Plateau endotherms, such as wild yaks (*Bos grunniens*), Tibetan plateau pika (*Ochotona curzoniae*), and ground tit (*Parus humilis*) cope with cold by producing sufficient energy via lipid metabolism and by retaining heat through compact coverings.[7–9] However, unfavorable conditions on the plateau pose great challenges for ectotherms given their dependence on environmental heat sources. Temperature sensing is a prerequisite for behavioral thermoregulation in ectotherms, which is critical for maintaining behavioral and physiological functions.[10] The ectothermic vertebrates have evolved the ability to exploit the spatiotemporal distribution of environmental temperatures to maximize energy utilization and survival.[11]

The ectothermic hot-spring snake (*Thermophis baileyi*), which is endemic to the QTP, shows a strong preference for habitats with hot springs as an adaptive strategy to climate change.[5,12–14] These snakes have the highest altitudinal distribution among reptiles, ranging from 3600 to 4900 m above sea level.[12] During the QTP uplift and ice age, ancestral populations of these snakes are thought to have found glacial refuges near geothermal resources and hot springs and may have evolved unique adaptive strategies to cope with the major geological and climatic events.[12] As such, these snakes provide an ideal opportunity to explore the genetic adaptations of ectotherms to extreme environments. We previously reported a draft genome of the hot-spring snake and revealed the molecular basis underlying UV and low-temperature adaptation.[15] However, the genetic basis of temperature acclimation and the adaptive changes in thermosensory systems in hot-spring snakes remain unknown. Notably, the relatively fragmented draft genomes reported thus far may introduce certain biases and miss key signals.[16]

Here, by integrating distributional information and behavioral comparisons, we revealed the preference of *T. baileyi* for hot-spring habitats and their rapid response to warm stimuli in cold environments, suggesting their thermosensory systems may have evolved to cope with temperature fluctuations. We also established a high-quality chromosome-level genome assembly of the hot-spring snake to gain insight into thermosensory and thermoregulatory adaptation. Comparative genomic analysis was performed to explore the evolutionary changes in coding genes and conserved non-coding elements, with a focus on the molecular basis of thermal perception. Genomic and experimental evidence showed significant evolutionary changes in temperature response, thermoregulation, and transient receptor potential (TRP) channel-related genes. Upon heating, *T. baileyi*-specific functional mutations in TRPA1 increased the heat-induced opening probability and thermal sensitivity of the ion channels, which may help in discovering suitable habitats more rapidly.

RESULTS

Hot-spring snakes prefer hot springs

We evaluated the preference of hot-spring snakes for hot-spring environments by integrating the distributional coordinates of both (supplemental Tables 1 and 2). As seen in the distribution map, the hot-spring snakes showed a preference for habitats with hot springs, with roughly half occurring in 40°C–60°C thermal springs (Figure 1A; supplemental Table 1).

It has been hypothesized that *T. baileyi* retreated to the micro-refugia created by hot springs and geothermal resources to survive changing climates, eg, during plateau uplift 20–60 million years ago.[12] As such, they may have evolved efficient temperature-perception capabilities and unique thermoregulation mechanisms to detect suitable habitats and cope with low temperatures and temperature fluctuations. Thus, we assessed and compared the ability of hot-spring snakes to detect ambient temperature by recording their choices of warm environments in response to cold stimulation (Figure 1B). Compared with other two snakes, hot-spring snakes demonstrated a strong preference for the high-temperature zone (*T. baileyi*, 80.56%, *Pantherophis guttatus*, 53.33%, *Pareas menglaensis*, 60.00%; Figure 1C). Furthermore, hot-spring

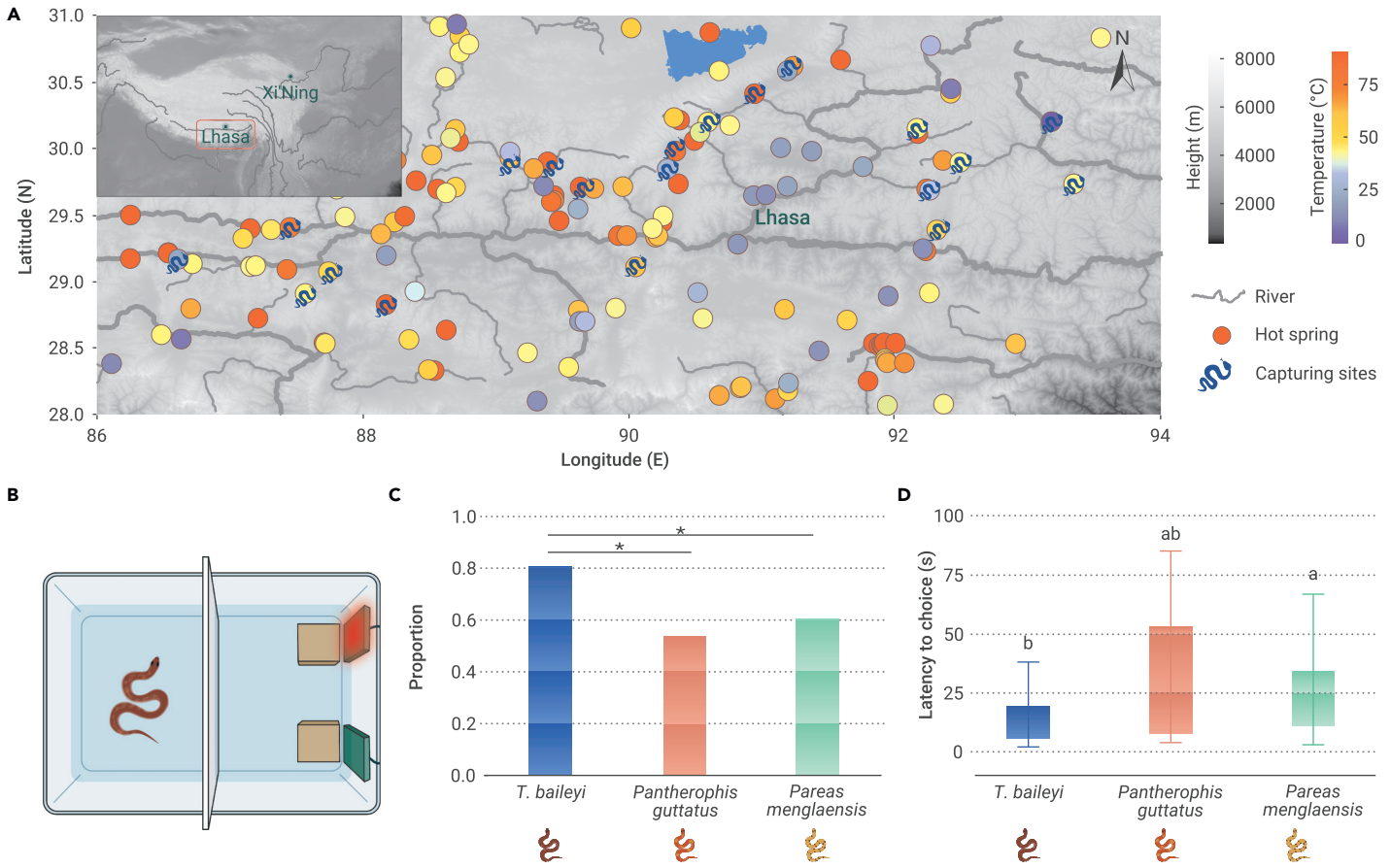

Figure 1. Distribution of *T. baileyi* and thermotropic behavior experiments (A) Geographical distribution of *T. baileyi* and hot springs on the QTP. Hot-spring temperatures are marked according to their highest records (supplemental Table 1). Distribution sites of *T. baileyi* are depicted with a snake. **(B)** The schematic diagrams of the setup for the behavioral test (top view). We put the snake in a plastic box (L × W × H: 66 × 47 × 40 cm), which is divided into two halves (adaptation area and selection area) by a dummy plate (white). Two identical stones (brown) in the selection area serve as resting places for the snakes. Two heating pads are on the two stones, against the wall. **(C)** The proportion of three kinds of snakes selecting high-temperature zone. *$P < 0.05$, exact binomial test. **(D)** The latency of three kinds of snakes selecting high-temperature zone. Kruskal-Wallis one-way analysis of variance on ranks, different superscript letters indicate significant differences among different treatments ($P < 0.05$). *T. baileyi*, n = 36; *Pantherophis guttatus*, n = 15; *Pareas menglaensis*, n = 30.

snakes located the warm environments more quickly (*T. baileyi*, 14.56 ± 10.86 s, *Pantherophis guttatus*, 30.53 ± 29.03 s, *Pareas menglaensis*, 24.6 ± 17.43 s; Figure 1D; supplemental Videos 1, 2, and 3). These findings suggest that *T. baileyi* may have evolved an efficient thermosensory system.

Genome assembly and chromosome evolution

In the current study, we sequenced the genome of a female hot-spring snake to explore the genetic changes in temperature-sensing systems using paired-end sequencing, single-molecule real-time sequencing, and Hi-C data (supplemental Table 3). A hybrid strategy (combined Illumina reads and PacBio long reads) was used to generate initial contigs, resulting in an assembly with a contig N50 of 4.02 Mb (supplemental Table 4) after polishing. The contigs were anchored onto chromosomes with Hi-C data, yielding a final chromosome-level assembly of 1.85 Gb with 91.47% of bases anchored onto 18 chromosomes (2n = 36) (Figure 2A and supplemental Figure 1). Based on Benchmarking Universal Single-Copy Ortholog (BUSCO) assessment of single-copy orthologous genes, genome completeness was 97.10% (supplemental Figure 2; supplemental Table 4). A total of 0.94 Gb of repetitive sequences were identified, accounting for 51.18% of the whole genome (supplemental Figure 3). We also annotated 22 292 coding genes. Compared with previously published snake genomes, the genome assembly was of relatively high quality (supplemental Figure 2; supplemental Tables 4 and 5).

Chromosome evolution is a fundamental driving force of evolution and is related to genome size, gene family evolution, and speciation.[17] Collinearity analysis found a high degree of collinearity within snakes but significant variation from birds and lizards (Figure 2B and supplemental Figure 4). Genes located within evolutionary breakpoint regions (EBRs) are associated with lineage-specific biology,[18–21] and 610 EBR genes were identified in *T. baileyi* (Figures 2C and 2D). Based on Gene Ontology (GO) enrichment analysis, we found that the EBR genes were significantly enriched in immune- and metabolism-related terms (supplemental Table 6). Furthermore, several genes were involved in DNA repair (eg, *PAXX*, *PARK7*, and *TAOK1*), hypoxia response (eg, *ENDOG*, *PSD10*, and *PSMD5*), and temperature acclimation (eg, *TRPC5*, *EHMT1*, *MFAP2*, and *WNT10*) (supplemental Table 7), suggesting that chromosome evolution in hot-spring snakes may be related to adaptation to high-altitude environments. However, the effects of chromosome evolution on the function of these genes and adaptive mechanisms of chromosome evolution in hot-spring snakes require further research.

Genome-wide convergent features within high-altitude lineages

Expansion to the QTP occurred independently in vertebrates. Here, we explored convergent molecular signals associated with high-altitude adaptation between high-altitude endotherms (eg, yaks, Tibetan plateau pika, and ground tit) and ectotherms (*T. baileyi* and *Nanorana parkeri*). Little molecular convergence was identified at the sequence level (convergent amino acid site), yet there was convergent acceleration in gene-wide rates of molecular evolution in these species. After setting high-altitude species as foreground branches, a total of 2109 genes were identified as common rapidly evolving genes. Among them, 72 were assigned in temperature-acclimation-related pathways or GO terms, including thermogenesis (k04714, P adjusted = 0.002), regulation of cellular response to heat (GO: 1900034, P adjusted = 0.001), negative regulation of cold-induced thermogenesis (GO: 0120163, P adjusted = 0.026), and positive regulation of cold-induced thermogenesis (GO: 0120162, P adjusted = 0.033) (Figure 3; supplemental Tables 8 and 9).

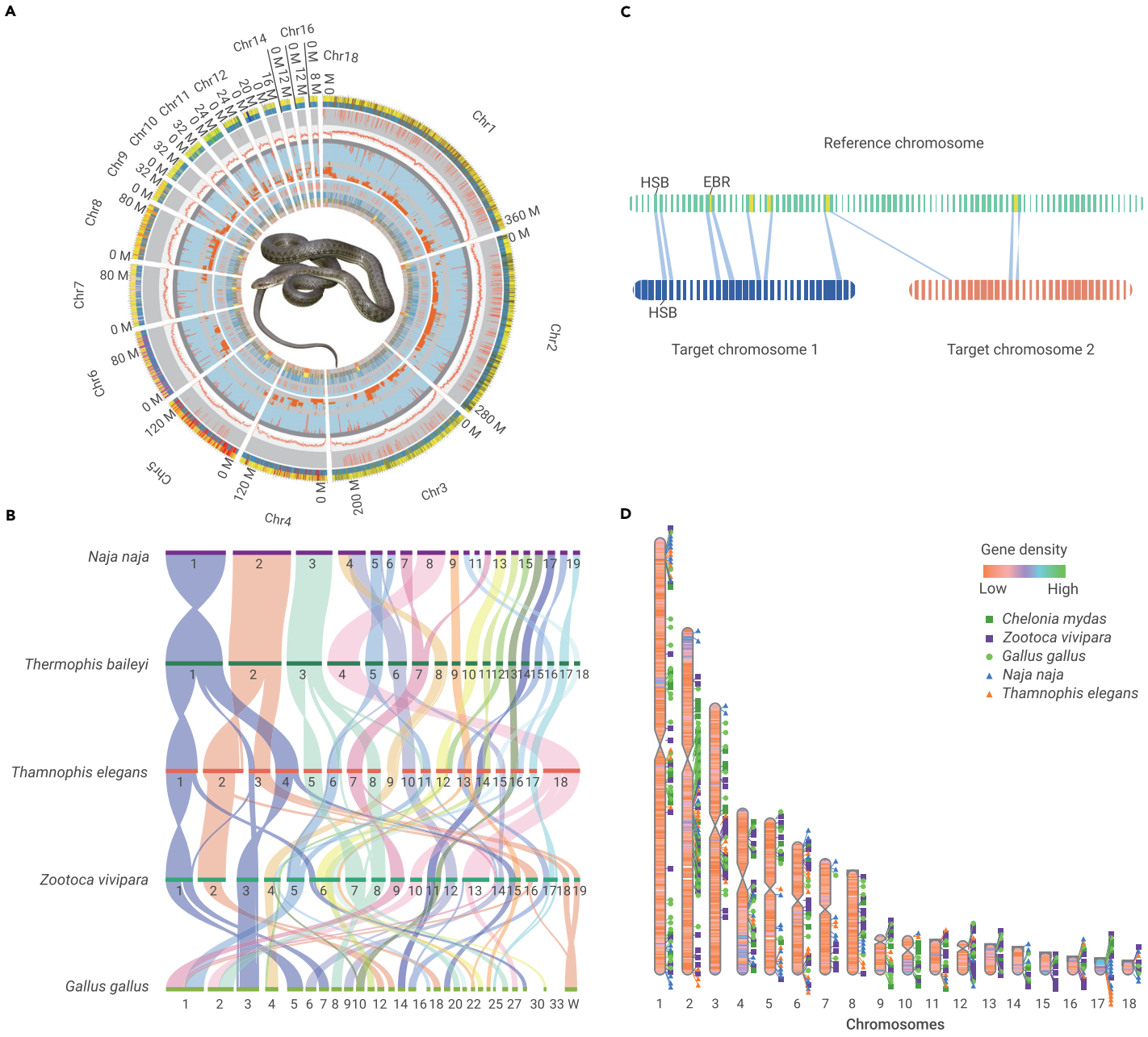

Figure 2. Chromosome evolution of *T. baileyi* genome (A) Circos plot of 18 chromosomes of *T. baileyi*. Protein-coding genes, highly divergent regions, GC-content, non-coding element regions, positively selected genes, and EBRs relative to *Thamnophis elegans*, *Zootoca vivipara*, and *Gallus gallus* are plotted on different levels of the circus from outer to inner. **(B)** Synteny tracker of genomes. Synteny regions are colored according to chromosome of *T. baileyi*. **(C)** Schematic of strategy to identify EBRs. An EBR was defined as an interval (in sulfur yellow) that is demarcated by the rearrangement of homology synteny blocks. **(D)** EBR distribution in *T. baileyi* genome. The color bands on the chromosome marks the gene density in *T. baileyi* genome.

Within these terms, *TRPM8* gene encodes a prototypical cold sensor in vertebrates, whose maximum cold activation is positively correlated with habitat temperature and is mainly determined by side-chain hydrophobicity and solvent accessibility in the pore domain.[22] Furthermore, many identified genes have thermogenic function, such as *Lpin1*, *Per2*, and *Lama4*, which are involved in cold response by regulating brown adipose tissue.[23–25] Brown adipose tissue is a unique thermogenic tissue in mammals,[26] thus the function of these thermogenesis-related genes in birds and ectotherms needs further investigation. In addition, several genes involved in hypoxia response and DNA repair were also identified (Figure 3; supplemental Tables 8 and 9). For instance, *Hus1*$^{-/-}$ cells show heightened sensitivity to UV light, implicating its function in the maintenance of genomic stability and UV response;[27] *AMAD12* and *AMAD17* are involved in hypoxia-induced impairment of neural vascular barrier function and are also considered as positively selected genes (PSGs) in yaks.[28,29] These genes are critical for high-altitude adaptation, allowing animals to cope with extreme environmental stresses, such as low temperatures, strong UV radiation, and hypoxia.

Evolutionary changes associated with thermosensation in *T. baileyi*

Ectothermic vertebrates can exploit the distribution of ambient heat to regulate their own temperature and survive,[11] which requires a sensitive thermosensory system. We performed comparative genomic analysis to explore the evolutionary changes in thermosensation- and thermoregulation-related genes. Here, we identified a set of 763 genes from 66 significantly expanded gene families (Figure 4A) involving basic biological processes, such as cold acclimation, cell differentiation, and development (supplemental Table 10). We then evaluated adaptive divergence in coding regions between hot-spring snakes and other Squamata species. A total of 1939 rapidly evolving genes (REGs) and 963 PSGs were detected in the

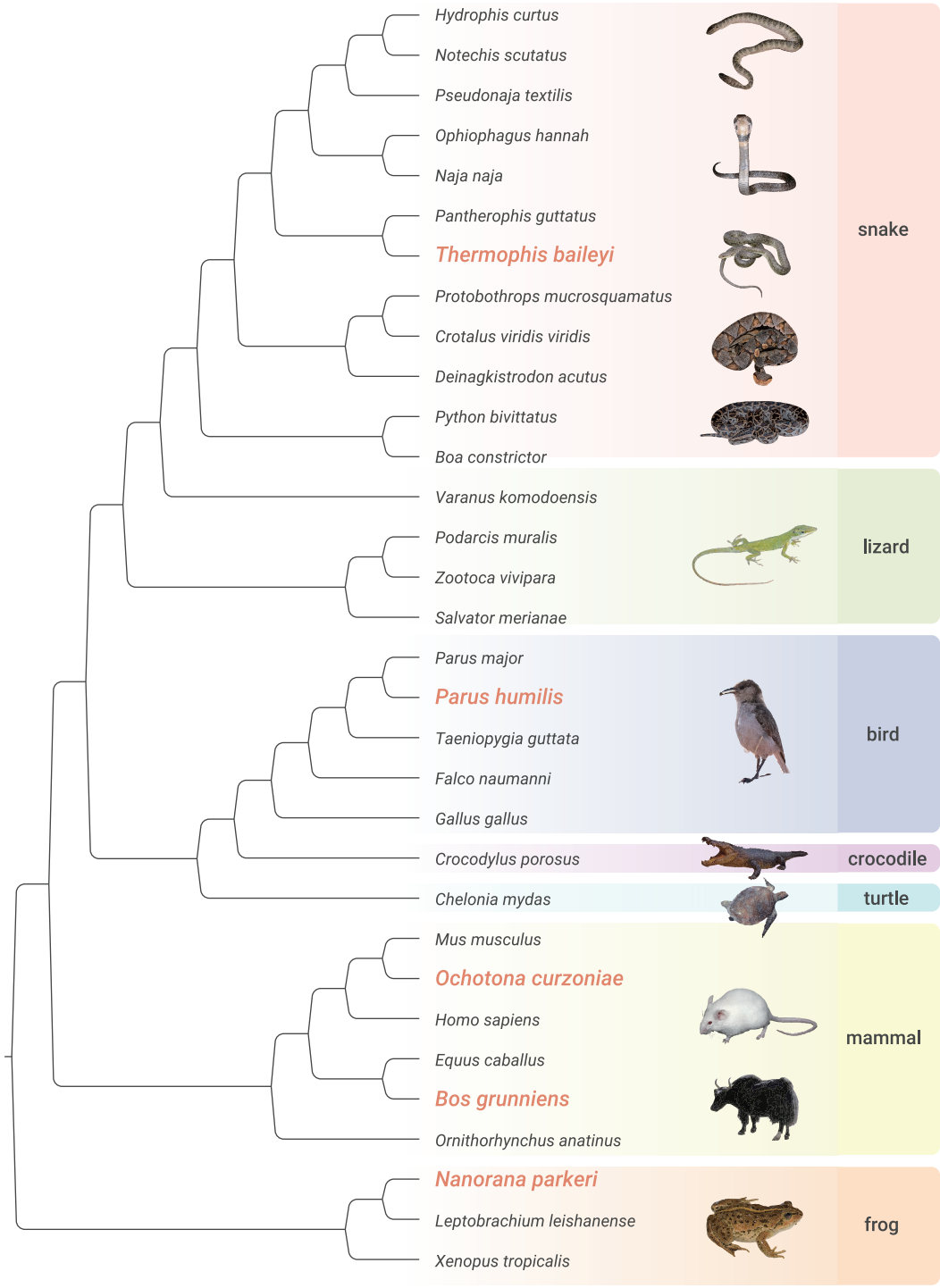

Temperature acclimation
GO:0120163: negative regulation of cold-induced thermogenesis
Corrected *P*-Value = 0.026
GO:0120162: positive regulation of cold-induced thermogenesis
Corrected *P*-Value = 0.033
GO:1900034: Regulation of cellular response to heat
Corrected *P*-Value = 0.001
K04714: Thermogenesis
Corrected *P*-Value = 0.002

Hypoxia response
GO:0001666: response to hypoxia
Corrected *P*-Value < 0.001
GO:0071456: cellular response to hypoxia
Corrected *P*-Value = 0.004

DNA damage repair
GO:0030838: Cellular response to UV
Corrected *P*-Value = 0.017
GO:0000724: double-strand break repair via homologous ecombination
Corrected *P*-Value < 0.001

Figure 3. Gene-wide convergent features of high-altitude species Five high-altitude species (orange) were set as foreground branches to detect rapidly evolving genes. Tree topology is supported by bootstrap supports of 100 for all nodes. The right panel is the Gene Ontology enrichment results.

hot-spring snake lineages using branch and branch-site models implemented in PAML.[30] In addition to several genes related to DNA repair and hypoxia adaptation, which support life at high elevation, a set of temperature-acclimation-related genes were also identified (supplemental Table 7).

Among the REGs, 28 were associated with temperature sensing and response (Figure 4B; supplemental Table 7). For example, TRPV3 is activated at warm temperature (33°C) and is responsible for thermotaxis, with this ability reported to be impaired in *TRPV3*$^{-/-}$ mice.[31,32] *CPB2* (*HSP47*) is involved in heat-stress responses,[33] and *HSF4* is required for induction of certain non-classic heat-shock genes.[34] Among the PSGs, nine were associated with temperature response (supplemental Table 7), eg, *CAMK2* is involved in the transmission of the signaling response to cold stress.[35,36] Taken together, the genes involved in thermosensation, thermotaxis, and heat/cold-stress response appear to have undergone adaptive changes, which may have contributed to species adaptation to the extreme plateau climate.

Evolution of temperature-sensing TRP channel genes

As TRP channel genes are considered important signal transducers for thermoreceptors,[37] we explored the features of all TRP channel genes in our analysis results. A total of 21 TRP channel genes were annotated in the genome, 12 of which exhibited *T. baileyi*-specific features (supplemental Table 11). In addition to the TRP channel genes mentioned above, *TRPC4AP*, *TRPC7*, and *TRPM1* showed

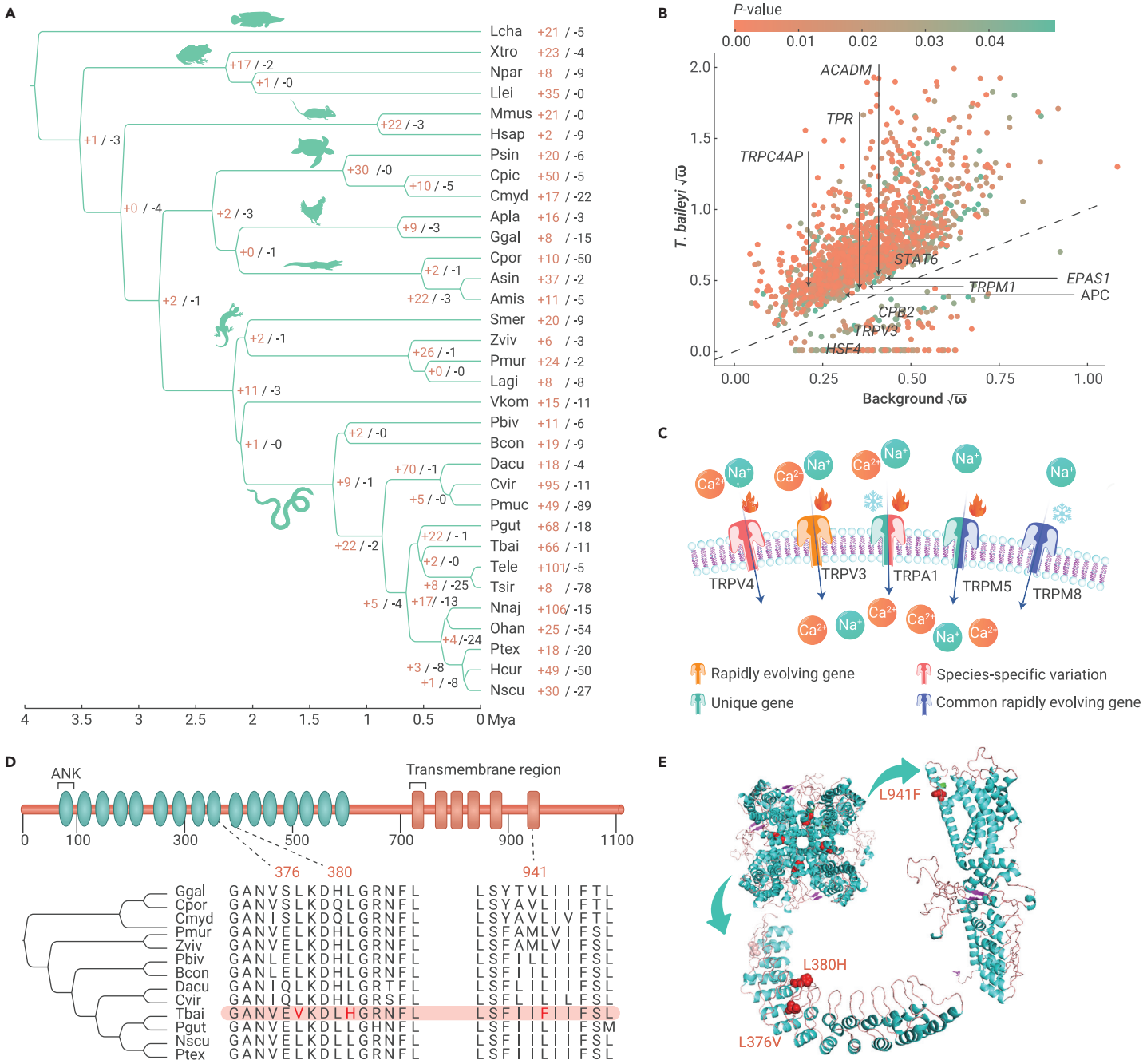

Figure 4. Molecular adaptation of *T. baileyi* to hot-spring habitats (A) Phylogenetic status of *T. baileyi* relative to other vertebrates. The number of significant expanded (orange) and contracted (black) gene families is designated on each node. The detailed species names are shown in the supplemental information. **(B)** Non-synonymous/synonymous substitution ratio (dn/ds) of *T. baileyi* temperature-sensing genes compared with background species. *P*-values of chi-square from likelihood ratio tests were marked in different colors. **(C)** Evolutionary changes in temperature-related TRP channel genes in hot-spring snake. **(D)** Protein alignment and variations of TRPA1. The distributions of three amino acid replacements are marked. **(E)** Three-dimensional structure of TRPA1 channel consists of four subunits. Red dots represent *T. baileyi*-specific replacements. The L941F is located on the TM6 domain, which is in proximity to the pore region of the homotetramer.

rapid evolution; *TRPA1*, *TRPC7*, *TRPM5*, and *TRPM7* were identified as *T. baileyi* unique genes; and *TRPV4AP* also showed positive selection. Furthermore, *T. baileyi*-specific replacements in *TRPV4* and *TRPA1* were identified. *TRPM7* is located in the 20 kb region up- and downstream of rapidly evolving non-coding elements, which were likely serve as proximal *cis*-regulatory elements.

Among these TRP channel genes, *TRPA1*, *TRPV4*, *TRPV3*, *TRPC5*, *TRPM5*, and *TRPM8* are temperature-sensing-related genes (Figure 4C, supplemental Table 11).[37] *TRPC5* and *TRPM8* are involved in cold sensation.[38,39] The TRP vanilloid (TRPV) channel family is activated by temperature,[40] and both TRPV3 and TRPV4 are activated under warm conditions (26°C–39°C).[37] TRPM5 is thought to be activated by warm temperature.[37] *TRPA1* is also a key molecular sensor involved in temperature detection.[37,41,42] As ion channels, TRPs can be gated directly and cause action potentials by sensory stimuli.[32] The extensive evolutionary changes in hot-spring snake TRP channel genes suggest adaptive changes in their perception systems, including thermosensation.

We next performed functional prediction to evaluate the role of species-specific replacements in TRPA1. Three *T. baileyi*-specific replacement sites were identified in the TRPA1 protein, which were found to be highly conserved in snakes (Figure 4D and supplemental Figure 5). Two replacements (L376V and L380H) were located on the intramembranous region of the transmembrane protein, ie, within the ninth and tenth ankyrin repeats domain (ANK). Another replacement (L941F) was located on the sixth membrane-spanning α-helical domain (transmembrane region 6 [TM6]) (Figures 4D and 4E). Two pore helices linked the fifth and sixth TM regions at the extracellular surface, which regulates cation influx.[43]

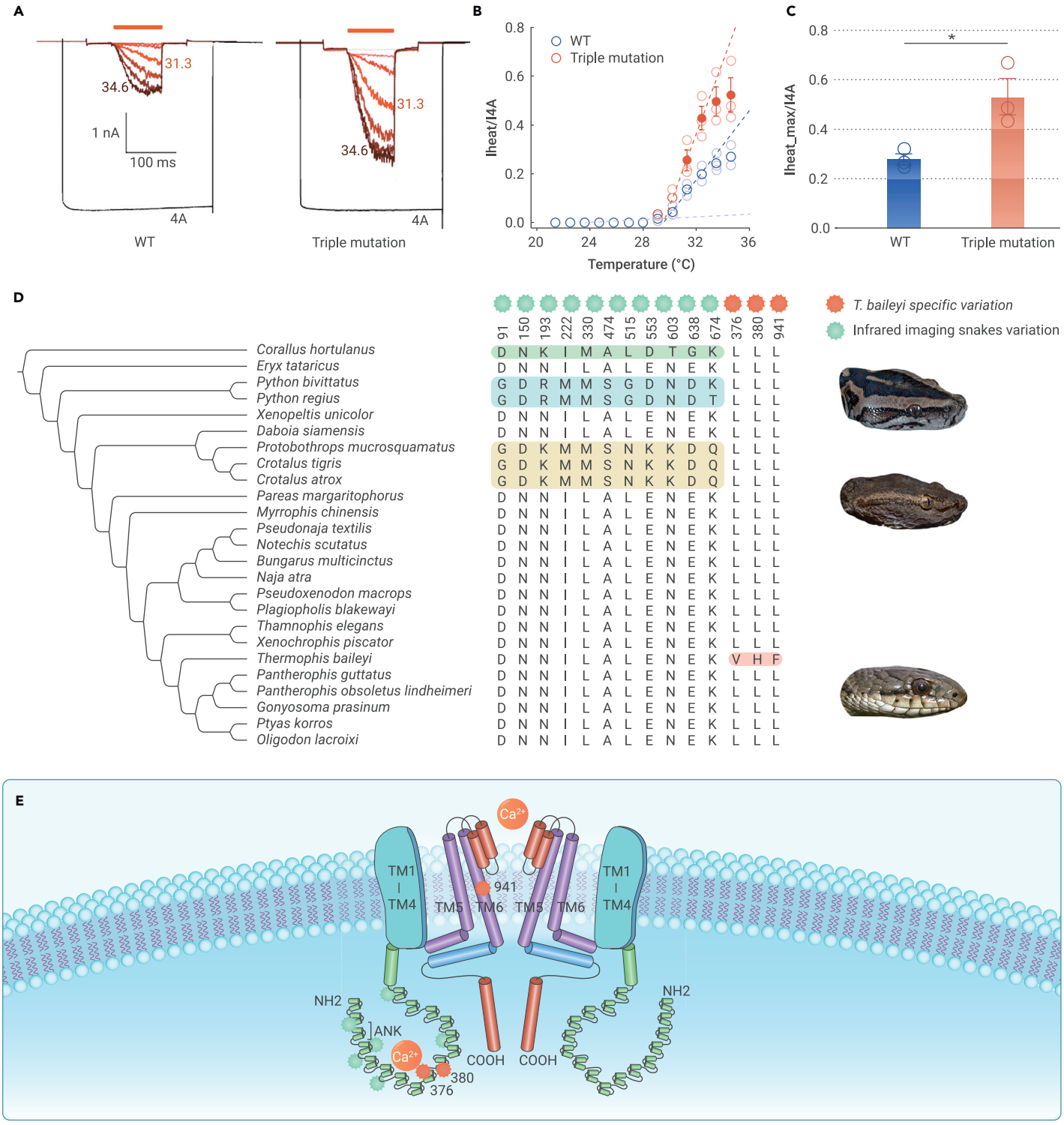

Figure 5. Laser-heating experiment and functional comparison of *T. baileyi* TRPA1 gene (A) Laser-induced heat activation of two types of TRPA1. 4-aminodiphe-nylamine is agonist of TRPA1. **(B)** Thermal activation curve of wild-type TRPA1 and mutant TRPA1. Channel activity was initially small and steadily increased with subsequent stimulations. Channel activity of two types of TRPA1 showed different growth rates. **(C)** Comparison of peak activity of two types of TRPA1. *$P < 0.01$. **(D)** Variation in TRPA1 among snakes. The alignment in the left block shows specific variation in infrared imaging snakes, and the right block shows specific variation in *T. baileyi*. **(E)** Schematic of TRPA1 transmembrane structure. TM1–TM6, transmembrane regions 1 to 6; ANK, Ankyrin repeats.

Three-dimensional structure prediction indicated that the structures between *Pantherophis guttatus* and *T. baileyi* were conserved (template modeling score >0.5) and the replacement sites may change the spatial conformation of TM5 and TM6, as well as the ANK "tail" (Figure S6). Functional prediction was performed using PROVEAN v.1.1.5 (Protein Variation Effect Analyzer),[44] which classified two replacements (L380H and L941F) as intolerant, suggesting that these replacements would likely result in functional changes in TRPA1 (Table S12). A *T. baileyi*-specific replacement (T500K) located on the ion transport domain of TRPV4 was also discovered (Figure S7). These results suggest that changes in thermotaxis- and temperature-response-related genes have occurred in hot-spring snakes, potentially providing powerful temperature detection and response capabilities to cope with extreme environments. Thus, we performed functional experiments to test how these changes affect the thermosensory system.

Laser-heating experiments and functional comparison of *TRPA1* gene

TRPA1 is a heat-sensitive ion channel and contributes to thermal detection and thermotaxis behavior in reptiles.[10,37,45] We performed electrophysiological and laser irradiation experiments to examine divergence between wild-type and mutant TRPA1 (ie, with three *T. baileyi*-specific replacements) in response to heat. Figure 5A shows the temperature responses of the two types of TRPA1 after repeated stimulation with different temperatures produced by laser irradiation.[46] The TRPA1 agonist (4-aminodiphe-nylamine) is potent against reptile TRPA1 orthologs,[10] activating the channel with a high probability of opening in the absence of heat (Figure 5A). Whole-cell recordings indicated that heat activation of TRPA1 was normalized to agonist-induced currents (Figure 5A). We found that the temperature threshold (~29°C–30°C) was comparable between the wild-type and mutated TRPA1 (Figure 5B). Subsequently, the peak currents of the wild-type and mutant channels significantly increased upon heating (Figure 5B). We then compared the current amplitudes at the end of each stimulus. Results showed that heat sensitivity of the TRPA1 mutant was higher than that of the wild type (Figure 5C). Functional analysis showed that the three *T. baileyi*-specific replacements in the TRPA1 did not alter the temperature-response threshold values but increased heat sensitivity to some extent.

The molecular mechanism of TRPA1 in thermal detection in hot-spring snakes may differ from that of snakes with pit organs. In infrared imaging snakes, TRPA1 shows an extremely robust response to infrared heat sources, mainly by lowering the thermal activity threshold.[45] Interestingly, the positions of the replacement sites in hot-spring snake differed from the specific amino acid replacements in infrared imaging snakes (Figure 5D). Most infrared imaging snake-specific sites are distributed in the N-terminal domain (ANK1 to TM1) (Figure 5E). Structural prediction suggests that their structures are conserved (template modeling score >0.5) but with spatial conformation differences within their ANK tail (supplemental Figure 8), suggesting a potential region responsible for infrared detection capacity.[47] The *T. baileyi*-specific amino acid replacements on TM6 may alter the conformation of the ion channel constructed by TM5 and TM6 and, in turn, alter the openness under the same temperature stimulus (Figures 5D and 5E; supplemental Figure 6). The other two replacements located within the ANK region may provide a cytoplasmic surface for interactions with ligands and conformational changes, thereby opening the channel.[43]

Genomic adaptation in other temperature-acclimation genes

Neural circuit mechanisms are critical for thermoregulation, acting as a signal carrier in thermosensation.[48] Here, we identified 2437 unique genes that overlapped with *T. baileyi*-unique regions, with several significantly enriched terms related to neurons and synapses (eg, neuron projection, nervous system development, synapse, and neuron projection morphogenesis) (supplemental Table 13). We also found that several genes regulated by divergent non-coding elements were associated with neurogenesis (eg, synapse assembly, nervous system development, and neuron development) (supplemental Table 14). These results indicate that the evolution of both coding and non-coding elements may have contributed to the physiological basis of temperature perception. Although hot springs provide microhabitats and environments suitable for *Thermophis* species, those with excessively high temperatures may be a risk. We identified several genes involved in the transmission of thermal pain-evoked signals, such as *PRDM12* (EBR gene) and *OPRK1* (PSG) (supplemental Table 7). Previous studies have shown that individuals with *PRDM12* mutations exhibit impaired noxious heat or cold pain sensitivity[49] and that *OPRK1* knockout mice exhibit enhanced thermal hyperalgesia.[50–52] Thus, hot-spring snakes may have evolved sensitive sensory systems to avoid harmful temperature stimuli.

DISCUSSION

The QTP is considered a "natural laboratory" for research on adaptations to extreme environments.[4,6] In this study, we demonstrated the thermal sensitivity of hot-spring snakes through behavioral experiments and discovered extensive evolutionary changes in genes associated with thermal adaptation based on a high-quality genome assembly. These findings were not detected in our earlier draft genome,[15] which was primarily due to the incompleteness of the assembly and annotation (eg, *TRPA1* and *TRPM8*). The improved high-quality genome provides an important genetic resource for studying the biological characteristics of this rare species.

Similar environmental stress may drive species to acquire convergent phenotypes or physiology. In this study, little convergent amino acid replacement was identified at sequence level, but convergent signatures of acceleration in gene-wide rates of molecular evolution were detected across high-altitude endotherms and ectotherms, including hypoxia response, cold response, and UV-induced DNA-damage repair, which are necessary to cope with extreme altitude environment. A study on the high-altitude domestic mammals found similar patterns: little convergent evolution at the DNA sequence level occurring among different high-altitude domestic mammals, but convergent signature of positive selection in genes associated with hypoxia response existed.[53] This suggests that although endotherms and ectotherms have very different physiological characteristics, they tend to change identical genes in order to respond to similar environmental stresses. Temperature-induced adaptation is often synergistic with physiological regulation,[11] which is conducive to cold acclimation. In this study, we identified several REGs, PSGs, and common REGs involved in thermogenesis. Some of these genes, such as *TBC1D7*, *UTP15*, and *GCLC* were also identified as PSGs in opah, a warm-blooded fish,[54] suggesting their role in thermal adaptations in vertebrates. However, the function of these genes has been elucidated only in endotherms, remaining unknown in ectothermic reptiles, especially the effects of cold-induced thermogenesis-related genes, and thus require further investigation.

Cold stress requires organisms to evolve sensitive thermal sensors and regulatory mechanisms, which is important for ectotherms that rely on environmental heat sources. TRP channels are an important class of molecules that contribute to thermosensation in vertebrates.[32,55] Here, extensive evolutionary changes in TRP channels were identified in hot-spring snakes, implying the evolution of their temperature-sensing system. TRPA1 mediates thermal detection and thermotaxis behavior.[10,37,45,56] Our results demonstrated that minimal changes in protein sequence (three amino acid replacements) are sufficient to generate a wide diversity of heat-induced opening probabilities and thermal sensitivities in TRPA1.[57] This finding is consistent with the behavioral experiments, which showed strong and sensitive thermotaxis in the hot-spring snakes. Furthermore, TRPA1 also mediates the perception of the rate of temperature change,[55] which may help organisms respond to temperature changes more quickly.

The differences in *TRPA1* mutations and function between *T. baileyi* and infrared imaging snakes further suggest the adoption of two distinct molecular-sensing strategies, one of which modulates the temperature-sensing range by reducing the minimum activation threshold (eg, infrared imaging snakes),[45] and the other of which adjusts heat-induced opening probability and thermal sensitivity of *TRPA1*, thus responding more quickly and sensitively to temperature changes. Structural variations of TRPA1 ion channel determine its diverse function and performance. We found that features between the two molecular-sensing strategies were mainly characterized by spatial conformation changes in ANK tail and TM5–TM6 domain. ANK tail is responsible for the diverse functions of proteins, such as ion transporters and signal transducers, and are important for the function of thermal nociception in *Drosophila*.[58,59] ANK can communicate with the pore and be responsible for thermal or chemical responsiveness.[60] The pore of TRPA1 is formed by the pore-forming helices in TM6 of the tetrameric channel, and point mutations in TM6 would reduce heat sensitivity.[61,62] Given that changes at the TRPA1 sequence level may mediate different response mechanisms, it is important to determine the functional consequences of TRPA1 mutations and associated physiological processes in future studies. Overall, evolutionary changes in the thermosensory system of hot-spring snakes may have contributed to their survival in hot-spring refuges under changing geological and climatic conditions, as well as their adaptation to high-altitude plateau environments under temperature fluctuation.

METHODS

Data and code availability

The genome assembly and raw sequencing data have been deposited in National Genomics Data Center (NGDC) (https://ngdc.cncb.ac.cn) under NGDC: PRJCA007342 (GWH: GWHBJWY00000000, GSA: CRA006131, GSA: CRA006150).

Experimental model and subject details

This study was approved by the Animal Ethics Committee of the CIB, and animal experiments were carried out in line with the institution's guidelines.

REFERENCES

1. Saito, S., and Tominaga, M. (2017). Evolutionary tuning of TRPA1 and TRPV1 thermal and chemical sensitivity in vertebrates. Temperature ***4***, 141–152.
2. Saito, S., Ohkita, M., Saito, C.T., et al. (2016). Evolution of heat sensors drove shifts in thermosensation between *Xenopus* species adapted to different thermal niches. J. Biol. Chem. ***291***, 11446–11459.
3. Laursen, W.J., Schneider, E.R., Merriman, D.K., et al. (2016). Low-cost functional plasticity of TRPV1 supports heat tolerance in squirrels and camels. Proc. Natl. Acad. Sci. USA ***113***, 11342–11347.
4. Wingfield, J.C., Patrick Kelley, J., Angelier, F., et al. (2011). Organism-environment interactions in a changing world: a mechanistic approach. J. Ornithol. ***152***, S279–S288.
5. Hofmann, S. (2012). Population genetic structure and geographic differentiation in the hot spring snake *Thermophis baileyi* (Serpentes, Colubridae): indications for glacial refuges in southern-central Tibet. Mol. Phylogenet. Evol. ***63***, 396–406.
6. Deng, T., Wu, F., Zhou, Z., and Su, T. (2020). Tibetan Plateau: an evolutionary junction for the history of modern biodiversity. Sci. China Earth Sci. ***63***, 172–187.
7. Li, J., Yang, Q., Bai, Z., et al. (2018). Chronic cold exposure results in subcutaneous adipose tissue browning and altered global metabolism in Qinghai-Tibetan plateau pika (*Ochotona curzoniae*). Biochem. Biophys. Res. Commun. ***500***, 117–123.
8. Jia, C., Wang, H., Li, C., et al. (2019). Genome-wide detection of copy number variations in polled yak using the Illumina BovineHD BeadChip. BMC Genom. ***20***, 376.
9. Qu, Y., Zhao, H., Han, N., et al. (2013). Ground tit genome reveals avian adaptation to living at high altitudes in the Tibetan plateau. Nat. Commun. ***4***, 2071.
10. Ye, Y.Z., Zhang, H., Li, J., et al. (2021). Molecular sensors for temperature detection during behavioral thermoregulation in turtle embryos. Curr. Biol. ***31***, 2995–3003.e4.
11. Hutchison, V.H., and Maness, J.D. (1979). The role of behavior in temperature acclimation and tolerance in ectotherms. Am. Zool. ***19***, 367–384.
12. Cloudsley-Thompson, J. (2007). The ecological specialist, *Thermophis baileyi* (Wall, 1907) – new records, distribution and biogeographic conclusions. Herpetol. Bull. ***101***, 8–12.
13. Huang, S., Liu, S.y., Guo, P., et al. (2009). What are the closest relatives of the hot-spring snakes (Colubridae, *Thermophis*), the relict species endemic to the Tibetan Plateau? Mol. Phylogenet. Evol. ***51***, 438–446.
14. Ren, J.-L., Yan, C., Peng, Z.-L., and Li, J.-T. (2022). Sichuan hot-spring snakes imperiled: reason, situation, and protection. Zool. Res. ***43***, 95–97.
15. Li, J.-T., Gao, Y.D., Xie, L., et al. (2018). Comparative genomic investigation of high-elevation adaptation in ectothermic snakes. Proc. Natl. Acad. Sci. USA ***115***, 8406–8411.
16. Mallick, S., Gnerre, S., Muller, P., and Reich, D. (2009). The difficulty of avoiding false positives in genome scans for natural selection. Genome Res. ***19***, 922–933.
17. Eichler, E.E., and Sankoff, D. (2003). Structural dynamics of eukaryotic chromosome evolution. Science ***301***, 793–797.
18. Farré, M., Kim, J., Proskuryakova, A.A., et al. (2019). Evolution of gene regulation in ruminants differs between evolutionary breakpoint regions and homologous synteny blocks. Genome Res. ***29***, 576–589.
19. Groenen, M.A.M., Archibald, A.L., Uenishi, H., et al. (2012). Analyses of pig genomes provide insight into porcine demography and evolution. Nature ***491***, 393–398.
20. Ullastres, A., Farré, M., Capilla, L., and Ruiz-Herrera, A. (2014). Unraveling the effect of genomic structural changes in the rhesus macaque - implications for the adaptive role of inversions. BMC Genom. ***15***, 530.
21. Farré, M., Narayan, J., Slavov, G.T., et al. (2016). Novel insights into chromosome evolution in birds, archosaurs, and reptiles. Genome Biol. Evol. ***8***, 2442–2451.
22. Yang, S., Lu, X., Wang, Y., et al. (2020). A paradigm of thermal adaptation in penguins and elephants by tuning cold activation in TRPM8. Proc. Natl. Acad. Sci. USA ***117***, 8633–8638.
23. Nadra, K., Médard, J.J., Mul, J.D., et al. (2012). Cell autonomous Lipin 1 function is essential for development and maintenance of white and Brown adipose tissue. Mol. Cell Biol. ***32***, 4794–4810.
24. Chappuis, S., Ripperger, J.A., Schnell, A., et al. (2013). Role of the circadian clock gene Per2 in adaptation to cold temperature. Mol. Metab. ***2***, 184–193.
25. Vaicik, M.K., Blagajcevic, A., Ye, H., et al. (2018). The absence of laminin a4 in male mice results in enhanced energy expenditure and increased beige subcutaneous adipose tissue. Endocrinology ***159***, 356–367.
26. Ballinger, M.A., and Andrews, M.T. (2018). Nature's fat-burning machine: Brown adipose tissue in a hibernating mammal. J. Exp. Biol. ***121***, 1–10.
27. Weiss, R.S., Enoch, T., and Leder, P. (2000). Inactivation of mouse Hus1 results in genomic instability and impaired responses to genotoxic stress. Genes Dev. ***14***, 1886–1898.
28. Qiu, Q., Zhang, G., Ma, T., et al. (2012). The yak genome and adaptation to life at high altitude. Nat. Genet. ***44***, 946–949.
29. Cui, D., Arima, M., Takubo, K., et al. (2015). ADAM12 and ADAM17 are essential molecules for hypoxia-induced impairment of neural vascular barrier function. Sci. Rep. ***5***, 12796.
30. Yang, Z. (2007). PAML 4: Phylogenetic analysis by maximum likelihood. Mol. Biol. Evol. ***24***, 1586–1591.
31. Moqrich, A., Hwang, S.W., Earley, T.J., et al. (2005). Impaired thermosensation in mice lacking TRPV3, a heat and camphor sensor in the skin. Science ***307***, 1468–1472.
32. Dhaka, A., Viswanath, V., and Patapoutian, A. (2006). TRP ion channels and temperature sensation. Annu. Rev. Neurosci. ***29***, 135–161.
33. Abdelnasir, A., Sun, J.R., Cheng, Y.F., et al. (2014). Evaluation of Hsp47 expression in heat-stressed rat myocardial cells in vitro and in vivo. Genet. Mol. Res. ***13***, 10787–10802.
34. Fujimoto, M., Oshima, K., Shinkawa, T., et al. (2008). Analysis of HSF4 binding regions reveals its necessity for gene regulation during development and heat shock response in mouse lenses. J. Biol. Chem. ***283***, 29961–29970.
35. Xu, D., You, Q., Chi, C., et al. (2018). Transcriptional response to low temperature in the yellow drum (*Nibea albiflora*) and identification of genes related to cold stress. Comp. Biochem. Physiol. Part D: Genomics Proteomics ***28***, 80–89.
36. Ju, Z., Dunham, R.A., and Liu, Z. (2002). Differential gene expression in the brain of channel catfish (*Ictalurus punctatus*) in response to cold acclimation. Mol. Genet. Genomics. ***268***, 87–95.
37. Xiao, R., and Xu, X.Z.S. (2021). Temperature sensation: from molecular thermosensors to neural circuits and coding principles. Annu. Rev. Physiol. ***83***, 205–230.
38. Brauchi, S., Orio, P., and Latorre, R. (2004). Clues to understanding cold sensation: thermodynamics and electrophysiological analysis of the cold receptor TRPM8. Proc. Natl. Acad. Sci. USA ***101***, 15494–15499.
39. Zimmermann, K., Lennerz, J.K., Hein, A., et al. (2011). Transient receptor potential cation channel, subfamily C, member 5 (TRPC5) is a cold-transducer in the peripheral nervous system. Proc. Natl. Acad. Sci. USA ***108***, 18114–18119.
40. Liu, B., Yao, J., Zhu, M.X., and Qin, F. (2011). Hysteresis of gating underlines sensitization of TRPV3 channels. J. Gen. Physiol. ***138***, 509–520.
41. Caspani, O., and Heppenstall, P.A. (2009). TRPA1 and cold transduction: an unresolved issue? J. Gen. Physiol. ***133***, 245–249.
42. Cortright, D.N., Krause, J.E., and Broom, D.C. (2007). TRP channels and pain. Biochim. Biophys. Acta ***1772***, 978–988.
43. Paulsen, C.E., Armache, J.P., Gao, Y., et al. (2015). Structure of the TRPA1 ion channel suggests regulatory mechanisms. Nature ***520***, 511–517.
44. Choi, Y., Sims, G.E., Murphy, S., et al. (2012). Predicting the functional effect of amino acid substitutions and indels. PLoS One ***7***, e46688.
45. Gracheva, E.O., Ingolia, N.T., Kelly, Y.M., et al. (2010). Molecular basis of infrared detection by snakes. Nature ***464***, 1006–1011.
46. Yao, J., Liu, B., and Qin, F. (2010). Kinetic and energetic analysis of thermally activated TRPV1 channels. Biophys. J. ***99***, 1743–1753.
47. Geng, J., Liang, D., Jiang, K., and Zhang, P. (2011). Molecular evolution of the infrared sensory gene TRPA1 in snakes and implications for functional studies. PLoS One ***6***, e28644.
48. Liedtke, W.B. (2017). Deconstructing mammalian thermoregulation. Proc. Natl. Acad. Sci. USA ***114***, 1765–1767.
49. Chen, Y.C., Auer-Grumbach, M., Matsukawa, S., et al. (2015). Transcriptional regulator PRDM12 is essential for human pain perception. Nat. Genet. ***47***, 803–808.
50. Palmisano, M., Caputi, F.F., Mercatelli, D., et al. (2019). Dynorphinergic system alterations in the corticostriatal circuitry of neuropathic mice support its role in the negative affective component of pain. Genes Brain Behav. ***18***, e12467.
51. Xu, M., Petraschka, M., McLaughlin, J.P., et al. (2004). Neuropathic pain activates the endogenous κ opioid system in mouse spinal cord and induces opioid receptor tolerance. J. Neurosci. ***24***, 4576–4584.
52. Aita, M., Byers, M.R., Chavkin, C., and Xu, M. (2010). Trigeminal injury causes kappa opioid-dependent allodynic, glial and immune cell responses in mice. Mol. Pain ***6***, 8.
53. Wu, D.D., Yang, C.P., Wang, M.S., et al. (2020). Convergent genomic signatures of high-Altitude adaptation among domestic mammals. Natl. Sci. Rev. ***7***, 952–963.
54. Wang, X., Qu, M., Liu, Y., et al. (2022). Genomic basis of evolutionary adaptation in a warm-blooded fish. Innovation ***3***, 100185.
55. Luo, J., Shen, W.L., and Montell, C. (2017). TRPA1 mediates sensation of the rate of temperature change in *Drosophila* larvae. Nat. Neurosci. ***20***, 34–41.
56. Corfas, R.A., and Vosshall, L.B. (2015). The cation channel TRPA1 tunes mosquito thermotaxis to host temperatures. Elife ***4***, e11750.
57. Jabba, S., Goyal, R., Sosa-Pagán, J.O., et al. (2014). Directionality of temperature activation in mouse TRPA1 ion channel can be inverted by single-point mutations in ankyrin repeat six. Neuron ***82***, 1017–1031.
58. Hwang, R.Y., Stearns, N.A., and Tracey, W.D. (2012). The ankyrin repeat domain of the TRPA protein painless is important for thermal nociception but not mechanical nociception. PLoS One ***7***, e30090.
59. Bork, P. (1993). Hundreds of ankyrin-like repeats in functionally diverse proteins: mobile modules that cross phyla horizontally? Proteins ***17***, 363–374.
60. Cordero-Morales, J.F., Gracheva, E.O., and Julius, D. (2011). Cytoplasmic ankyrin repeats of transient receptor potential A1 (TRPA1) dictate sensitivity to thermal and chemical stimuli. Proc. Natl. Acad. Sci. USA ***108***, E1184–E1191.
61. Meents, J.E., Ciotu, C.I., and Fischer, M.J.M. (2019). Trpa1: a molecular view. J. Neurophysiol. ***121***, 427–443.
62. Wang, H., Schupp, M., Zurborg, S., and Heppenstall, P.A. (2013). Residues in the pore region of *Drosophila* transient receptor potential A1 dictate sensitivity to thermal stimuli. J. Physiol. ***591***, 185–201.

ACKNOWLEDGMENTS

We thank Hussam Zaher (University of São Paulo) for his advices on languages. We thank Chang-Jun Peng (Chengdu Institute of Biology, Chinese Academy of Sciences) for assistance with data analysis. We thank Jin-Long Ren (Chengdu Institute of Biology, Chinese Academy of Sciences) for his help in fieldwork. This work was supported by the Strategic Priority Research Program of Chinese Academy of Sciences (CAS) (XDB31000000); the National Natural Science Foundation of China (32100396); the Second Tibetan Plateau

Scientific Expedition and Research Program (STEP) (2019QZKK0501); Biodiversity Survey, Monitoring and Assessment Project of Ministry of Ecology and Environment, The People's Republic of China, China (2019HB2096001006); Key Research Program of Frontier Sciences, CAS (QYZDB-SSW-SMC058); the International Partnership Program of Chinese Academy of Sciences (151751KYSB20190024); and the Sichuan Science and Technology Program (2021JDJQ0002; 2021YJ0088).

AUTHOR CONTRIBUTIONS

J.-T.L. initiated and conceived the current work. C.Y., W.W., and Y.L., completed omics data analysis. W.D., and S.Y., performed the electrophysiology and laser irradiation experiments. B.Z. performed the behavioral experiments. J.C. provided important suggestions. W.W., C.Y., B.Z., and J.-T.L. wrote the manuscript, with input from all authors.

DECLARATION OF INTERESTS

The authors declare no competing interests.

SUPPLEMENTAL INFORMATION

Supplemental information can be found online at https://doi.org/10.1016/j.xinn.2022.100295.

LEAD CONTACT WEBSITE

http://sourcedb.cib.cas.cn/zw/rck/201303/t20130318_3795275.html.

The Innovation, Volume *3*

Supplemental Information

Temperature acclimation in hot-spring snakes and the convergence of cold response

Chaochao Yan, Wei Wu, Wenqi Dong, Bicheng Zhu, Jiang Chang, Yunyun Lv, Shilong Yang, and Jia-Tang Li

Supplementary Information:

The supplemental file includes:
Materials and Methods
Figures S1–S8
Tables S1–S6, S11, S12, S14, S15
Captions for Tables S7–S10, S13 (.xlsx)
Supplementary Videos S1-S3

Materials and Methods

Behavioral experiments and distribution information collection

The three snakes used in the experiment are of similar body length (*Thermophis baileyi*, 48.56 ± 14.71 cm; *Pantherophis guttatus*, 52.3 ± 12.3 cm; *Pareas menglaensis*, 45.3 ± 5.27 cm). To prevent interference from the surrounding heat, we wrapped the plastic experiment box in tin foil. Pure water at a low temperature (16.34 ± 2.22 ℃) was placed inside the box. After placing the snake into the adaptation zone, we removed the dummy plate, and recorded snake choices (preference) and latency (time to snakes arriving at resting stone). We considered the subjects to have made a choice only if they remained on the selected stone for more than 30 s. The entire process was video-recorded using a mobile phone. Each snake was tested three times and the heating pad was randomized in each test. The central temperature of the heating pad was 36.13 ± 1.84 ℃. After each test, the chamber was cleaned with 75% alcohol to eliminate residual odors. A total of 12 *T. baileyi*, five *P. guttatus*, and 10 *P. menglaensis* were used for behavioral experiments. Information on the distribution of snakes was collected from voucher specimens deposited at the Herpetological Museum, Chengdu Institute of Biology,

Chinese Academy of Sciences (Chengdu, China) and from published data (Table S1, S2).[1–5]

Genome sequencing and assembly

Blood tissue from the *T. baileyi* female that used to generate our previous draft genome[6] was used here to produce long reads. Whole genomic DNA was isolated and used to construct continuous long reads (CLR) DNA libraries with insert-size lengths of ~30 kb. The libraries were sequenced on a PacBio Sequel II sequencer. For *de novo* assembly of the *T. baileyi* genome, we first assembled initial contigs using short-read sequencing data, resulting in library insert sizes of 280 bp and 500 bp Illumina (~120 ×) by Platanus v1.2.4[7] with optimized parameters (-k 31 -t 8 -d 0.3 -m 200). Subsequently, the initial contigs were aligned to PacBio long reads (~180 ×) to construct contigs using DBG2OLC.[8] Base errors in the contigs were then polished based on PacBio long reads and Illumina short-reads using NextPolish v1.0.4.[9] BUSCO v5.1.3[10] was used to estimate the completion of the assembled genome.

Chromosome construction with Hi-C data

Liver tissue from a female hot-spring snake was sent to Anoroad Genome (Yiwu, China), where DNA was extracted and replicate Hi-C sequencing libraries were prepared. A total of 200 Gb of Hi-C data were produced at the Novogene Company (Tianjing, China) on two separate lanes of the Illumina HiSeq 4000 platform using 150-bp paired-end reads. Clean Illumina paired-end reads were mapped to the assembled

genome to construct a Hi-C map using the Juicer pipeline,[11] with binning at multiple resolutions (150, 500, and 1 000 kb).[12] Genome assembly quality was evaluated using BUSCO v5.1.3 with parameters -l vertebrata_odb10 -m genome -c 20 --limit 10.

Gene structural and functional annotations

Transcriptome data from a previous study were used for protein-coding gene (PCG) annotation.[6] Repeat elements were annotated and masked in the updated reference genome before gene model annotation. We applied Tandem Repeats Finder and RepeatMasker v4.1.0 for *ab initio* prediction of repeat elements in the genome.[13] Gene annotation was performed on the repetitive element-masked genome. Homology-, *ab initio*-, and transcriptome-based gene prediction methods were then used. The protein sequences of relative snake genomes were downloaded from Ensembl. Proteins from closely related snake species (*Naja naja*, *Ophiophagus hannah*, *Thamnophis elegans*, and *Pantherophis guttatus*) were mapped to the updated genome for homology prediction. Functional annotations of the PCGs were applied using BlastP-annotated proteins against the NR (non-redundant protein sequences in NCBI), SwissProt, and RefSeq databases (evalue < 1e-5). The NR BlastP results were processed using Blast2GO v5.2.5[14] to retrieve associated Gene Ontology (GO) terms describing biological processes, molecular functions, and cellular components (evalue < 1e-5). Kyoto Encyclopedia of Genes and Genomes (KEGG) KO and mapping information of each gene was obtained using the KOBAS v3.0.3 database.[15] The motifs and domains of each gene model were predicted by InterProScan against ProDom, PRINTS, Pfam,

Gene3D, CCD, SMART, PANTHER, PROSITE, and SUPERFAMILY.

Genome-wide convergent analysis

Orthofinder v2.2.7was used to identify single-copy gene families in *T. baileyi* and 31 other species with Markov clustering(MCL) inflation parameter set as 3 (Table S15).[16] Single gene clusters were then extracted and translated using self-made python scripts and the protein sequences from each family were aligned using prank v.150803 (http://wasabiapp.org/software/prank) with default parameters.[17] The alignments were trimmed with trimAl v1.4 in automated1 mode, and columns with gaps more than 0.5 and samples with more than 50% unusable sites were filtered.[18] DNA alignments were back translated according to the corresponding trimmed protein alignments using self-made scripts. The branch model of CODEML in PAML4.9[19] was used to test for potentially common rapidly evolving genes among high-altitude species. High-altitude species living in the QTP, i.e., *T. baileyi*, *N. parkeri*, *B. grunniens*, *O. curzoniae* and *P. humilis*, were set as the foreground branches and others as background branches. The null hypothesis was that the ω of each branch was equal (model = 0), while the alternative hypothesis allowed more than one ω (model = 2) across branches. The *P*-values were calculated based on the likelihood ratio test (LRT) for each model with chi-square test, with *P*-value < 0.01 representing significant common rapidly evolving genes

Gene family analysis

Orthologous groups of 33 species (Table S15) were constructed using OrthoFinder

v2.2.7.[16] Four-fold degenerate sites in the coding sequences (CDS) alignments were extracted with self-made scripts. All four-fold degenerate sites were then concatenated by species and used for phylogenomic analysis. A maximum-likelihood tree was constructed using IQ-TREE v 1.6.5[20] with parameters: -nt 10 -st DNA -bb 1000 -alrt 1000. Divergence time of species in the tree were calculated with MCMCTREE in PAML4.9[19]. Three divergence times, including that between ancestors of *Xenopus tropicalis* and *Homo sapiens*, between ancestors of *Homo sapiens* and *Mus musculus* and between ancestors of *Homo sapiens* and *Gallus gallus* were set according to the TimeTree website resource (http://www.timetree.org). Gene family expansion and contraction analyses were performed using CAFE v4.2.1.[21] Expanded and contracted gene families on each branch of the tree were detected by comparing the cluster size of each branch with the maximum-likelihood cluster size of the ancestral node leading to that branch; a small ancestral node indicated gene family expansion, whereas a large ancestral node indicated gene family contraction. The overall *P*-value (family-wide *P*-value in CAFE v4.2.1 based on 10,000 Monte Carlo resampling) was used to estimate the significant size variation for each gene family. For each branch or node, the exact *P*-value was calculated with Viterbi method to identify lineage-specific significantly varied gene families (overall *P*-value < 0.01).

Positively selected genes (PSGs) and rapidly evolving genes (REGs)

To identify potential PSGs and REGs in the *T. baileyi* genome, we used single-copy genes belonging to *T. baileyi* and 15 other species (i.e., *Pseudonaja textilis*,

Pantherophis guttatus, *Ophiophagus hannah*, *Python bivittatus*, *Crotalus viridis viridis*, *Notechis scutatus*, *Deinagkistrodon acutus*, *Naja naja*, *Boa constrictor*, *Hydrophis curtus*, *Podarcis muralis*, *Zootoca vivipara*, *Chelonia mydas*, *Crocodylus porosus*, and *Gallus gallus*) (Table S15). The branch-site model of CODEML in PAML v4.9[19] was used to test for potential PSGs, with *T. baileyi* set as the foreground branch and others set as background branches. The branch and site models were set to 2. In the null hypothesis, the ω value of each site on each branch was fixed to 1, whereas the alternative hypothesis was that the ω values of particular sites on the foreground branch were not fixed. The REGs are genes responsible for rapid divergence among taxa.[22] To identify REGs, we used the branch model, in which the alternative model allows different rates for different branches. The null hypothesis was that the ω of each branch was equal (model = 0), while the alternative hypothesis allowed more than one ω (model = 2) across branches. Chi-Square χ^2 and *P*-value for the likelihood ratio test were then determined following the CODEML processes. According to Bayes Empirical Bayes analysis, PSGs were defined based on a corrected *P*-value < 0.05 and at least one positively selected site with a posterior probability > 0.95.

Lineage-species mutations and unique genomic regions

Linage-species mutation was considered associated with lineage-specific adaptive characteristics.[23] To identify genes with species-specific mutations or unique regions in *T. baileyi*, we extracted sequences from 11-row alignments produced by multiz (v 11.2), with *T. baileyi* as the reference(Table S15). A self-made python script was then prepared to identify species-specific mutations and unique regions, referring to a previous study.[24] We defined *T. baileyi*-specific sequences as unique regions if they satisfied the following three criteria: 1) were only found in *T. baileyi*; 2) did not align with other lineages; 3) were located in the reconstructed genome of the most recent common ancestor (MRCA) of *T. baileyi*. The *T. baileyi*-specific mutations were screened from the alignment. To detect unique genes that evolved in *T. baileyi*, we first selected genes that overlapped with the *T. baileyi* lineage-specific sequence by more than 8 bp, which is longer than 99% of all unique regions, and the unique region are overlapped within exons or adjacent region (+2 bp or -2 bp) between exons and introns. We further evaluated the significance of unique regions enriched in the corresponding genes with a permutation test implemented in R package regioneR v1.18.1.[25] For each unique gene, 100 permutations were performed to get the unique genes with *P*-value < 0.01.

Chromosome synteny and evolutionary breakpoint regions (EBRs)

The PCGs were first used to construct a chromosome evolutionary landscape with the JCVI v1.1.11 utility libraries for python (https://github.com/tanghaibao/jcvi). Firstly,

orthologous proteins between two species were confirmed with the jcvi.compara.catalog module and block subsets were built based on the anchor file, which contained the genomic coordinates of each gene. The relationships of each block were visualized with the jcvi.graphics.karyotype module. Whole-genome synteny blocks were also identified with pipelines implemented in the mySyntenyPortal.[26] Whole-genome alignment of *T. baileyi* and other species was built with Lastz_D v1.03 (https://github.com/lastz/lastz). Homology synteny blocks (HSBs) were estimated with makeBlocks implemented in DESCHRAMBLER with resolution set as 100 kb.[27] We used a self-made script to identify EBRs between two adjacent HSBs based on the following criteria: 1) corresponding adjacent HSBs were in different target chromosomes; 2) adjacent HSBs in target chromosomes were broken by DNA fragments longer than 100 kb; 3) one adjacent HSBs was reversed in the target chromosomes. The EBR genes were defined as genes within 20-kb regions of the EBR flanks. The EBRs were visualized in chromosomes with the R package RIdeogram.

Rapidly evolving conserved non-coding elements (CNEs)

The genomes of 12 species (Table S15) were used to identify CNEs. The genome of *T. baileyi* was set as the reference. The other genomes were aligned to the reference using lastz_D. The MAF format files were further built into colinear alignment chains using axtChain (https://github.com/ucscGenomeBrowser/kent), followed by the net process using chainNet implemented in multiz. We removed low-scoring alignment nets with false homologies based on nets < 4 kb and scores < 20,000 with a span in both the

reference and query genomes. Multiz[28] was used to build multiple alignments, taking the filtered pairwise alignment nets as input. The phylogenetic position of the species selected was taken from our phylogenomic tree.

To compute local and global identity percentages between the CNE sequences of species and reconstructed ancestors as well as species and all common ancestors,[29] we used phylogeny aware PRANK v.150803 aligner with parameters "-keep -showtree -showanc -prunetree -seed 10", with the species tree assigned with the -t parameter. We determined the sequence identity percentage between the aligned ancestral sequence and CNE sequence of each species using the python module ete3[29]. The "Forward Genomics" generalized least square (GLS) approach[30] was used to identify significantly more-diverged CNEs in the *T. baileyi* genome (parameters: –thresholdConserved=0) and to compute the significance of associations between sequence-divergence and phenotypes. We set *T.baileyi* as the ingroup with 'pheno' set to 0, while the other species set as the outgroup. CNEs for which sequence identity values could not be calculated for *T. baileyi* were filtered. CNEs with GLS *P*-values < 0.05 were retained.

GO and KEGG enrichment analysis and structural prediction

GO enrichment analysis was performed using the R package clusterProfiler v4.0.1[31]. All annotated genes were set as background, while GO terms were obtained through annotation pipelines (see above). A hypergeometric test was performed to obtain the *P*-value for each GO term, and the Benjamini-Hochberg false discovery rate (FDR) multiple-test was then calculated. GO terms with a corrected *P*-value < 0.05 were

considered significantly enriched. Functional prediction was performed using PROVEAN v1.1.5 (Protein Variation Effect Analyzer), mutation was classified as deleterious if PROVEAN score less than -2.5.[33] Domain architectures of TRPA1 and TRPV4 were explored with SMART (https://smart.embl-heidelberg.de/). 3D protein structure was calculated with alphafold v2.0.0 in casp14 model with max_template_date set to 2000-05-14.[32] The topological similarity of protein structures were assessed with template modeling score (TM-Score).[34]

Laser irradiation experiments

We followed the laser irradiation protocols of Liu et al. (2011). Firstly, HEK293T cells were cultured in Dulbecco's modified Eagle medium with 10% fetal bovine serum and 1% penicillin/streptomycin, then incubated at 37 °C for 12–24 h with 5% CO_2. Transfection was performed using Lipofectamine 2000 (Life Technologies, USA) following the manufacturer's protocols. Green fluorescent protein (eEGFP) was transfected for laser beam pointing. Experiments were performed 24 h after transfection. We then synthesized the TRPA1 sequence of the corn snake, and the sequence of the corn snake with hot-spring snake-specific replacements. Patch-clamp recordings were used to record whole-cell and excised patch configurations, with sampling at 10–20 kHz. Laser irradiation was used to produce temperature jumps, which increased the temperature quickly and created a gradient.[35] The driving power of the laser was adjusted to produce junction potential measured at different temperatures.

References:

1. Liao, Z. (2018). Thermal Springs and Geothermal Energy in the Qinghai-

Tibetan Plateau and the Surroundings (Springer Hydrogeology).
2. Hofmann, S., Kraus, S., Dorge, T., et al. (2014). Effects of Pleistocene climatic fluctuations on the phylogeography, demography and population structure of a high-elevation snake species, *Thermophis baileyi*, on the Tibetan Plateau. J. Biogeogr. *41*, 2162–2172.
3. Huang, S., Liu, S. Y., Guo, P., et al. (2009). What are the closest relatives of the hot-spring snakes (Colubridae, *Thermophis*), the relict species endemic to the Tibetan Plateau? Mol. Phylogenet. Evol. *51*, 438–446.
4. Peng, L., Lu, C., Huang, S., et al. (2014). A new species of the genus *Thermophis* (Serpentes: Colubridae) from shangri-la, Northern Yunnan, China, With a proposal for an eclectic rule for species delimitation. Asian Herpetol. Res. *5*, 228–239.
5. Tong, W., Liao, Z., and Liu, S. (1999). Thermal Springs in Tibet (Science press).
6. Li, J.T., Gao, Y.D., Xie, L., et al. (2018). Comparative genomic investigation of high-elevation adaptation in ectothermic snakes. Proc. Natl. Acad. Sci. U. S. A. *115*, 8406–8411.
7. Kajitani, R., Toshimoto, K., Noguchi, H., et al. (2014). Efficient de novo assembly of highly heterozygous genomes from whole-genome shotgun short reads. Genome Res. *24*, 1384–1395.
8. Ye, C., Hill, C.M., Wu, S., et al. (2016). DBG2OLC: Efficient assembly of large genomes using long erroneous reads of the third generation sequencing technologies. Sci. Rep. *6*, 31900.
9. Hu, J., Fan, J., Sun, Z., and Liu, S. (2020). NextPolish: A fast and efficient genome polishing tool for long-read assembly. Bioinformatics *36*, 2253–2255.
10. Waterhouse, R.M., Seppey, M., Simao, F.A., et al. (2018). BUSCO applications from quality assessments to gene prediction and phylogenomics. Mol. Biol. Evol. *35*, 543–548.
11. Durand, N.C., Shamim, M.S., Machol, I., et al. (2016). Juicer Provides a One-Click System for Analyzing Loop-Resolution Hi-C Experiments. Cell Syst. *3*, 95–98.
12. Jacob M. D., Janies, D., Brouwer, C., and Grant, T. (2018). A new strategy to infer circularity applied to four new complete frog mitogenomes. Ecol. Evol. *8*, 4011–4018.
13. Jiang, W., Lv, Y., Cheng, L., et al. (2019). Whole-Genome Sequencing of the Giant Devil Catfish, *Bagarius yarrelli*. Genome Biol. Evol. *11*, 2071–2077.
14. Conesa, A., and Götz, S. (2008). Blast2GO: A comprehensive suite for functional analysis in plant genomics. Int. J. Plant Genomics *2008*, 619832.
15. Bu, D., Luo, H., Huo, P., et al. (2021). KOBAS-i: Intelligent prioritization and exploratory visualization of biological functions for gene enrichment analysis. Nucleic Acids Res. *49*, W317–W325.
16. Emms, D.M., and Kelly, S. (2019). OrthoFinder: Phylogenetic orthology inference for comparative genomics. Genome Biol. *20*, 1–14.
17. Russell, D.J. (2014). Methods in Molecular Biology: Multiple sequences

alignment Methods (Humana press).
18. Capella-Gutiérrez, S., Silla-Martínez, J.M., and Gabaldón, T. (2009). trimAl: A tool for automated alignment trimming in large-scale phylogenetic analyses. Bioinformatics *25*, 1972–1973.
19. Yang, Z. (2007). PAML 4: Phylogenetic analysis by maximum likelihood. Mol. Biol. Evol. *24*, 1586–1591.
20. Nguyen, L.T., Schmidt, H.A., Von Haeseler, A., and Minh, B.Q. (2015). IQ-TREE: A fast and effective stochastic algorithm for estimating maximum-likelihood phylogenies. Mol. Biol. Evol. *32*, 268–274.
21. Han, M.V., Thomas, G.W.C., Lugo-Martinez, J., and Hahn, M.W. (2013). Estimating gene gain and loss rates in the presence of error in genome assembly and annotation using CAFE 3. Mol. Biol. Evol. *30*, 1987–1997.
22. Dapper, A.L., and Wade, M.J. (2020). Relaxed Selection and the Rapid Evolution of Reproductive Genes. Trends Genet. *36*, 640–649.
23. Cotney, J., Leng, J., Yin, J., et al. (2013). The Evolution of Lineage-Specific Regulatory Activities in the Human Embryonic Limb. Cell *154*, 185–196.
24. Feng, S., Stiller, J., Deng, Y., et al. (2020). Dense sampling of bird diversity increases power of comparative genomics. Nature *587*, 252–257.
25. Gel, B., Díez-Villanueva, A., Serra, E., et al. (2016). RegioneR: An R/Bioconductor package for the association analysis of genomic regions based on permutation tests. Bioinformatics *32*, 289–291.
26. Lee, J., Lee, D., Sim, M., et al. (2018). mySyntenyPortal: An application package to construct websites for synteny block analysis. BMC Bioinformatics *19*, 1–7.
27. Kim, J., Farré, M., Auvil, L., et al. (2017). Reconstruction and evolutionary history of eutherian chromosomes. Proc. Natl. Acad. Sci. U. S. A. *114*, E5379–E5388.
28. Aguirre-Mesa, A.M., Garcia, M.J., and Millwater, H. (2020). MultiZ: A Library for Computation of High-order Derivatives Using Multicomplex or Multidual Numbers. ACM Trans. Math. Softw. *46*, 23–30.
29. Prudent, X., Parra, G., Schwede, P., et al. (2016). Controlling for Phylogenetic Relatedness and Evolutionary Rates Improves the Discovery of Associations between Species' Phenotypic and Genomic Differences. Mol. Biol. Evol. *33*, 2135–2150.
30. Hiller, M., Schaar, B.T., Indjeian, V.B., et al. (2012). A "Forward Genomics" Approach Links Genotype to Phenotype using Independent Phenotypic Losses among Related Species. Cell Rep. *2*, 817–823.
31. Wu, T., Hu, E., Xu, S., et al. (2021). clusterProfiler 4.0: A universal enrichment tool for interpreting omics data. Innov. *2*, 100141.
32. Jumper, J., Evans, R., Pritzel, A., et al. (2021). Highly accurate protein structure prediction with AlphaFold. Nature *596*, 583–589.
33. Choi, Y., Sims, G.E., Murphy, S., et al. (2012). Predicting the Functional Effect of Amino Acid Substitutions and Indels. PLoS One *7*, e46688.
34. Xu, J., and Zhang, Y. (2010). How significant is a protein structure similarity

with TM-score = 0.5? Bioinformatics *26*, 889–895.
35. Yao, J., Liu, B., and Qin, F. (2010). Kinetic and energetic analysis of thermally activated TRPV1 channels. Biophys. J. *99*, 1743–1753.

Supplementary Figures:

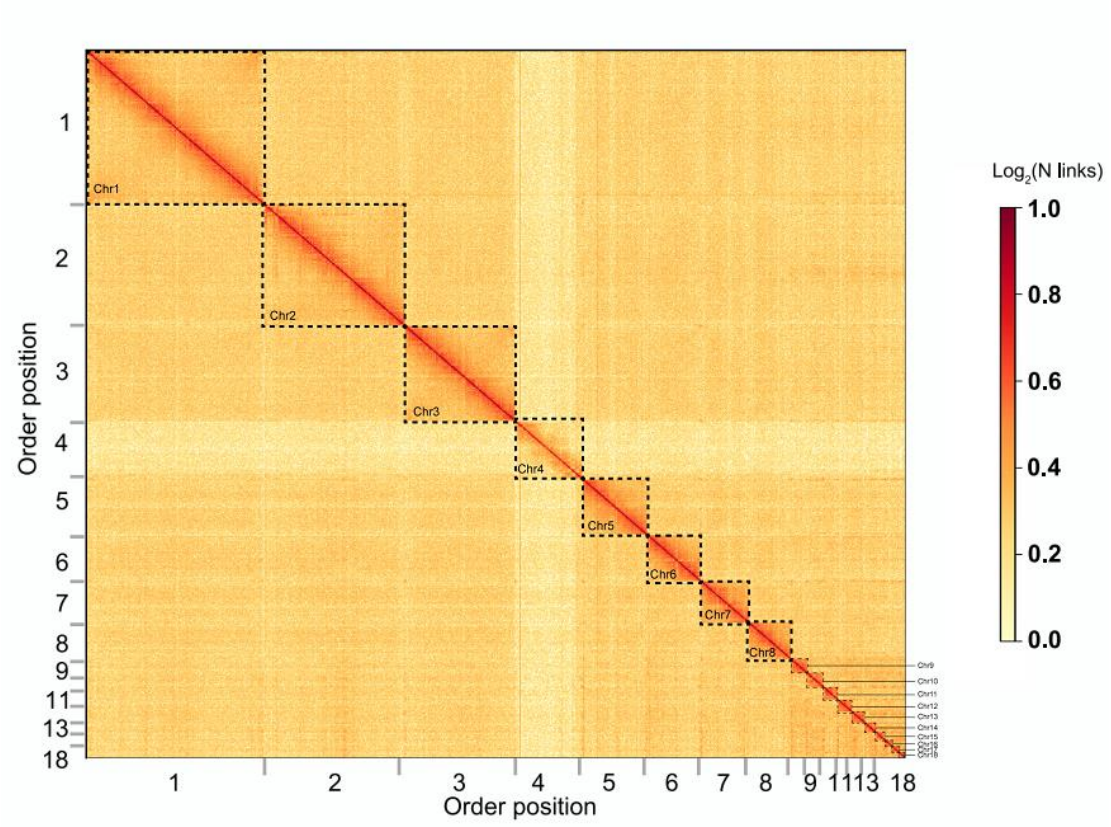

Figure S1. Heat map of chromosomal contacts in *T. baileyi* chromosomes at 500 kb resolution. The fourth cluster (chr4) showing less interaction with other chromosomes is sex chromosome Z.

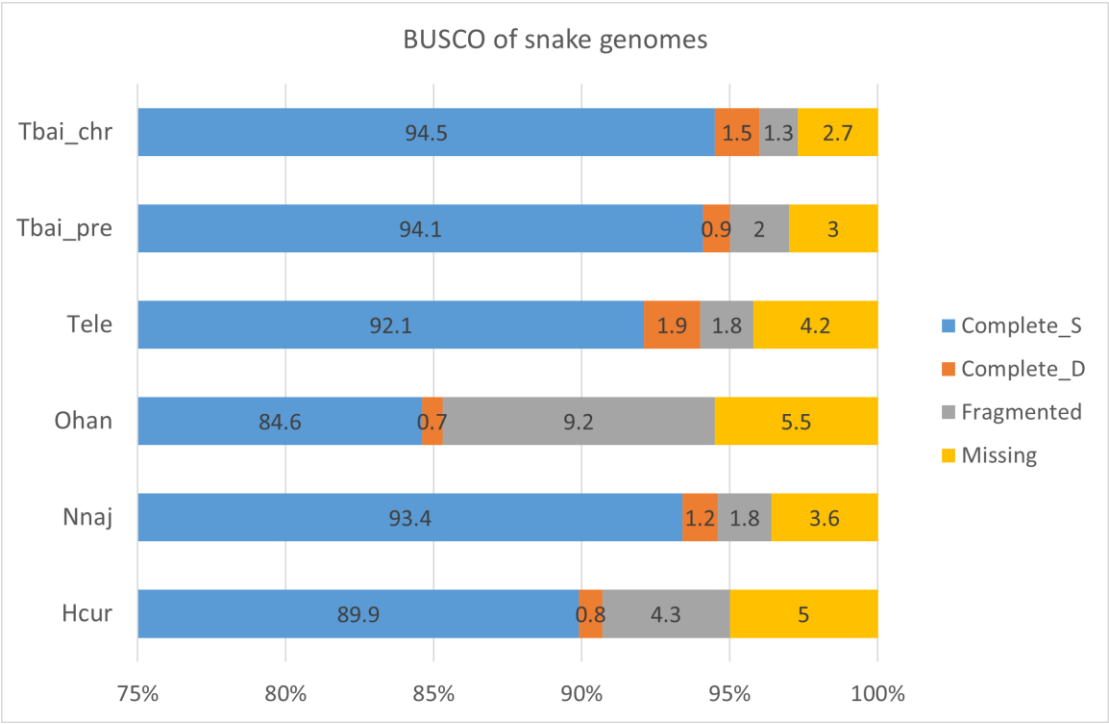

Figure S2. BUSCO assessment of snake genome completeness. Tbai_pre: previous version *T. baileyi* genome; Tbai_chr: *T. baileyi* genome in this study; Tele: *Thamnophis elegans*; Ohan: *Ophiophagus hannah*; Nnaj: *Naja naja*; Hcur: *Hydrophis curtus*.

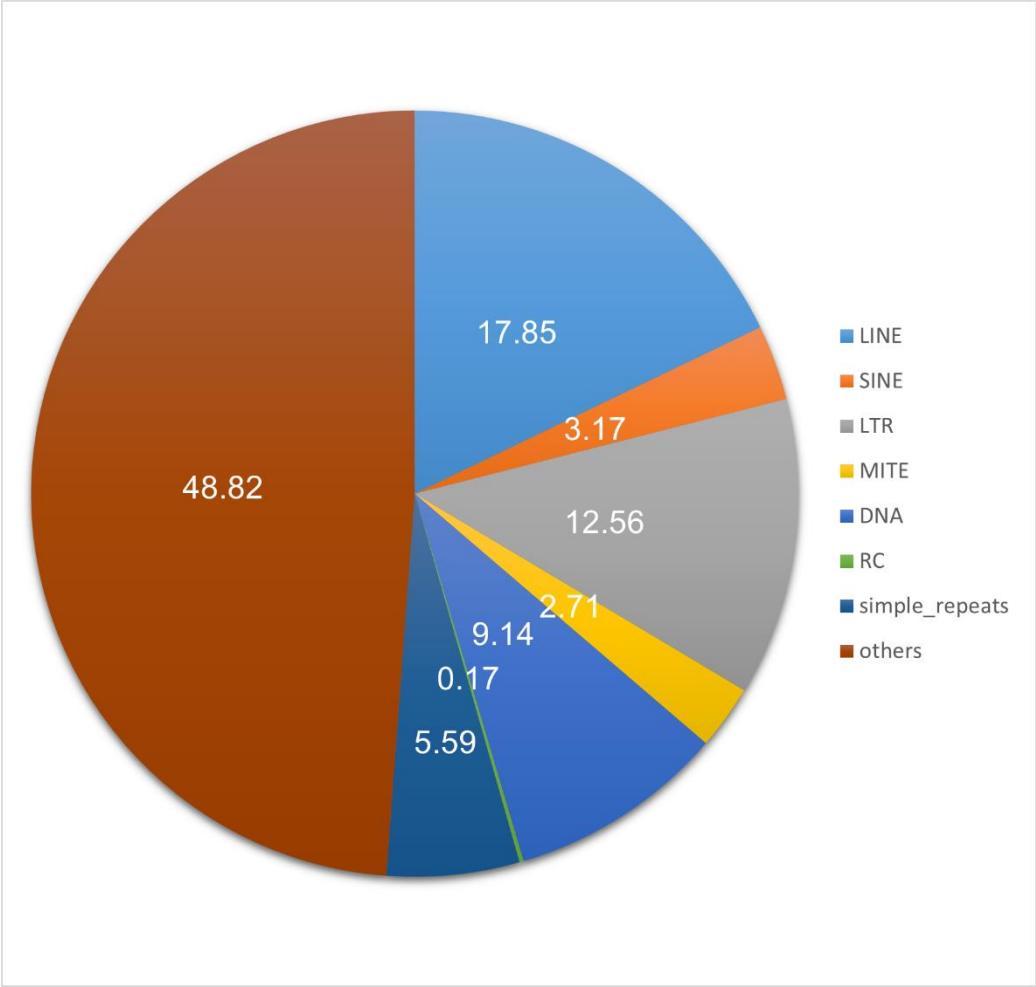

Figure S3. Sequence composition of *T. baileyi* genome. Repetitive sequences occupy 51.18% of the whole genome. The "others" represents non-repetitive sequences. The "simple_repeats" represents all other repeat sequences in addition to those of Class I (retrotransposons) and Class II (DNA transposons).

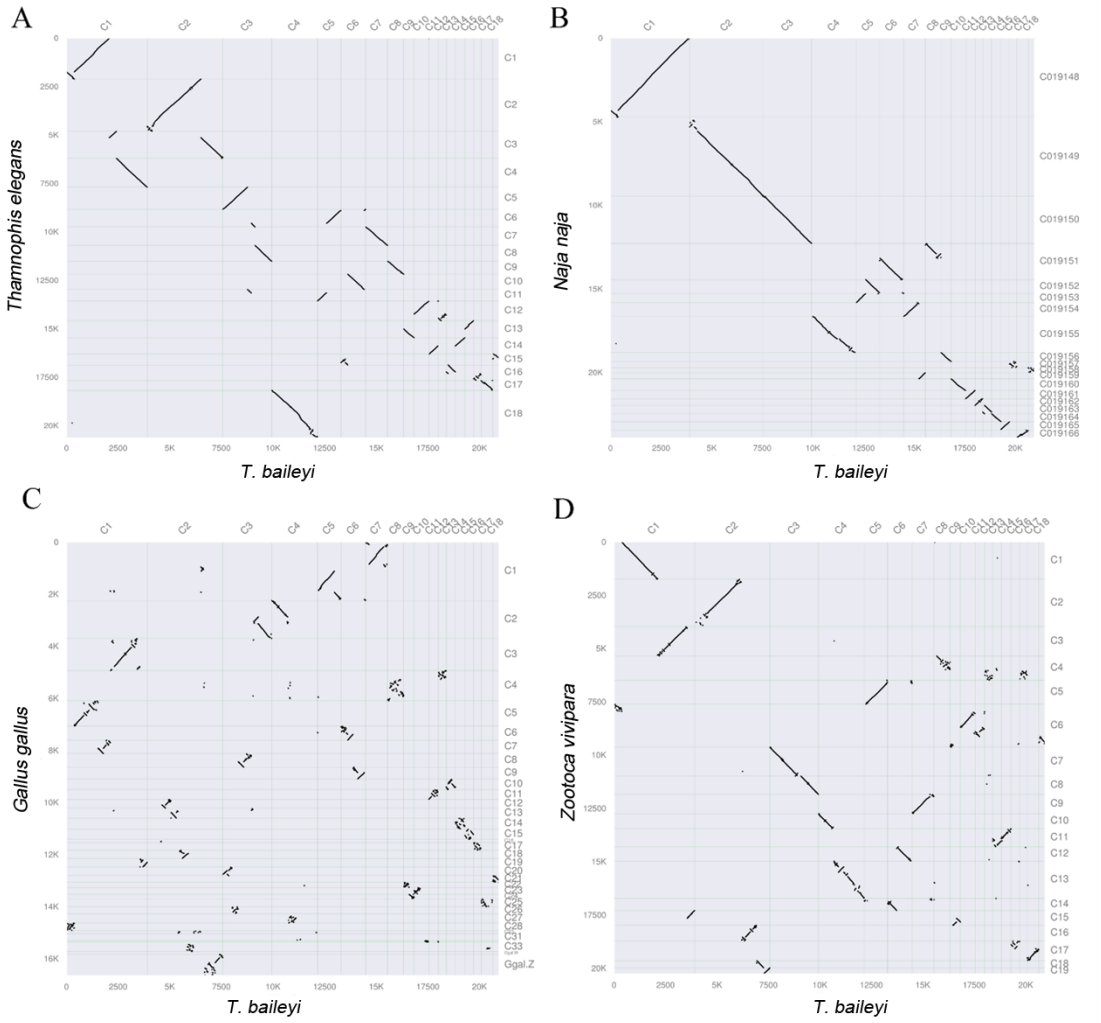

Figure S4. Protein-coding gene-based synteny plots between *T. baileyi* and other vertebrates. Intergenomic comparisons between (A) *T. baileyi* and *Thamnophis elegans*, 15 742 genes were paired. (B) *T. baileyi* and *Naja naja*, 14 701 genes were paired. (C) *T. baileyi* and *Gallus gallus*, 12 416 genes were paired. (D) *T. baileyi* and *Zootoca vivipara* 15 297 genes were paired.

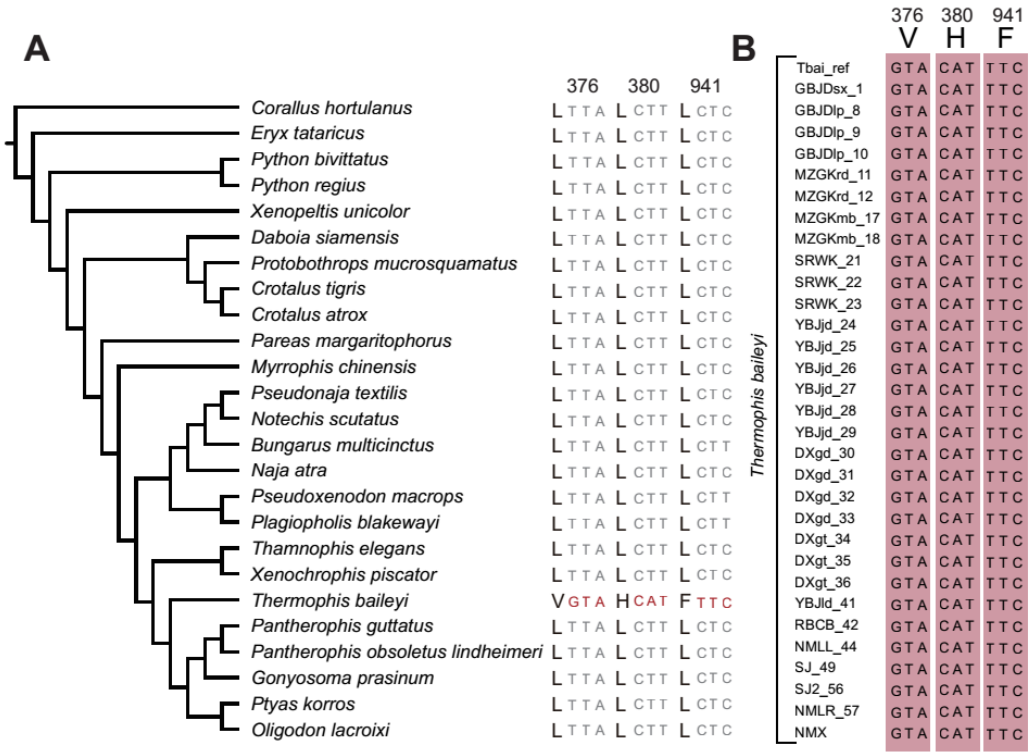

Figure S5. (A) The three TRPA1 mutations (L376V, L380H and L941F) and corresponding nucleotide mutations in *T. baileyi* relative to other snakes. (B) The hot-spring snake-specific TRPA1 replacements are confirmed by 31 *T. baileyi* whole genome re-sequencing data (unpublished data in another manuscript, accession number: CRA005375).

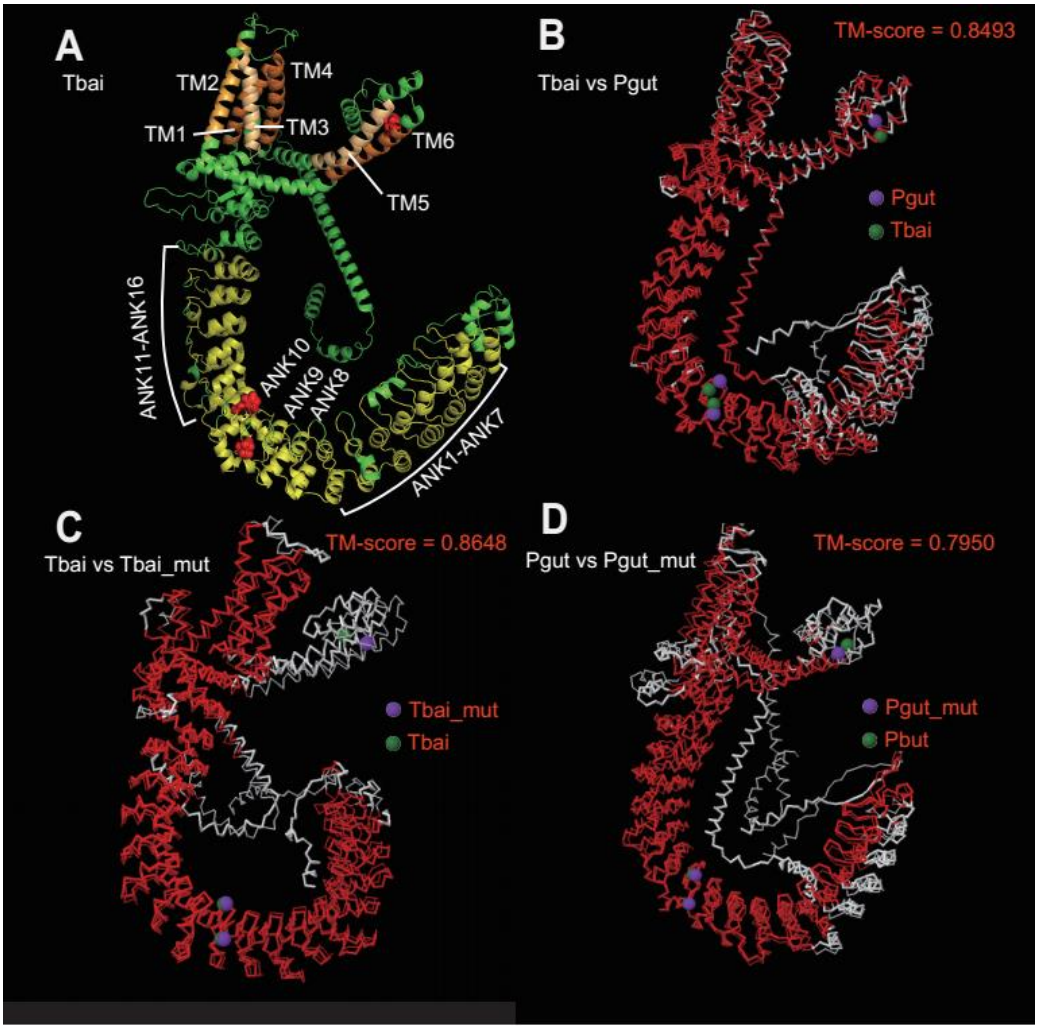

Figure S6. 3D structural modification of TRPA1 associated with the three *T. baileyi* specific variations. (A**)** 3D structure of *T. baileyi* TRPA1 predicted by Alphafold2, the 16 ANK domains were in yellow, and the 6 TM domains were in orange and light orange, the names of the domains were marked around these functional domains. **(**B) superposition of TRPA1 between *T. baileyi* (Tbai, in thick wireframes) *and Pantherophis guttatus* (Pgut, in thin wireframes). The structure of TRPA1 between the two species is conserved. (C) superposition of TRPA1 between *T. baileyi* with three artificial back variations (Tbai_mut, in thin wireframes) and original *T. baileyi* TRPA1 protein (in thick wireframes). The replacement site in TM6 may alter the spatial conformation of TM5 and TM6. (D) superposition of TRPA1 between *P. guttatus* (in thick wireframes) and *P. guttatus* with the three *T. baileyi* specific variations (Pgut_mut, in thin wireframes). The replacement sites may alter the spatial conformation of TM5 and TM6, as well as ANK "tail". The TM-score of these superpositions were depicted on the left top, and residues with d < 5Å in are in red, and the amino acid loci of *T. baileyi* specific amino acid variation were marked with green and purple circles.

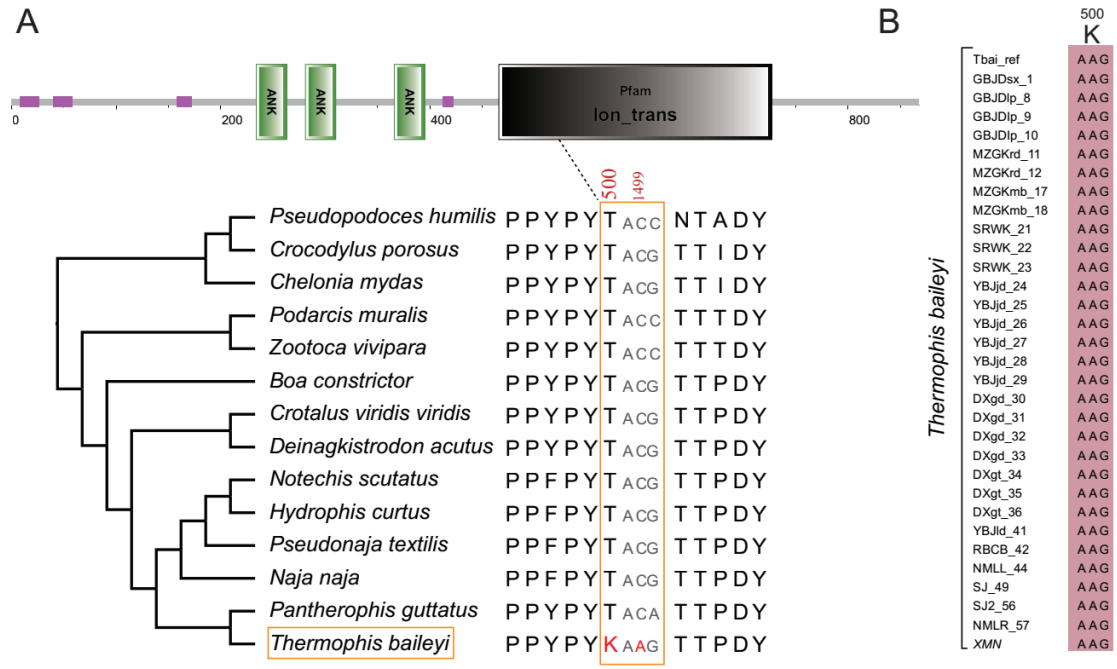

Figure S7. *T. baileyi*-specific variation in TRPV4 genes. (A) The T500K replacement specifically occurred in *T. baileyi* was caused by the C1499A mutation. (B) The hot-spring snake-specific T500K replacement was confirmed by 31 *T. baileyi* whole genome re-sequencing data.

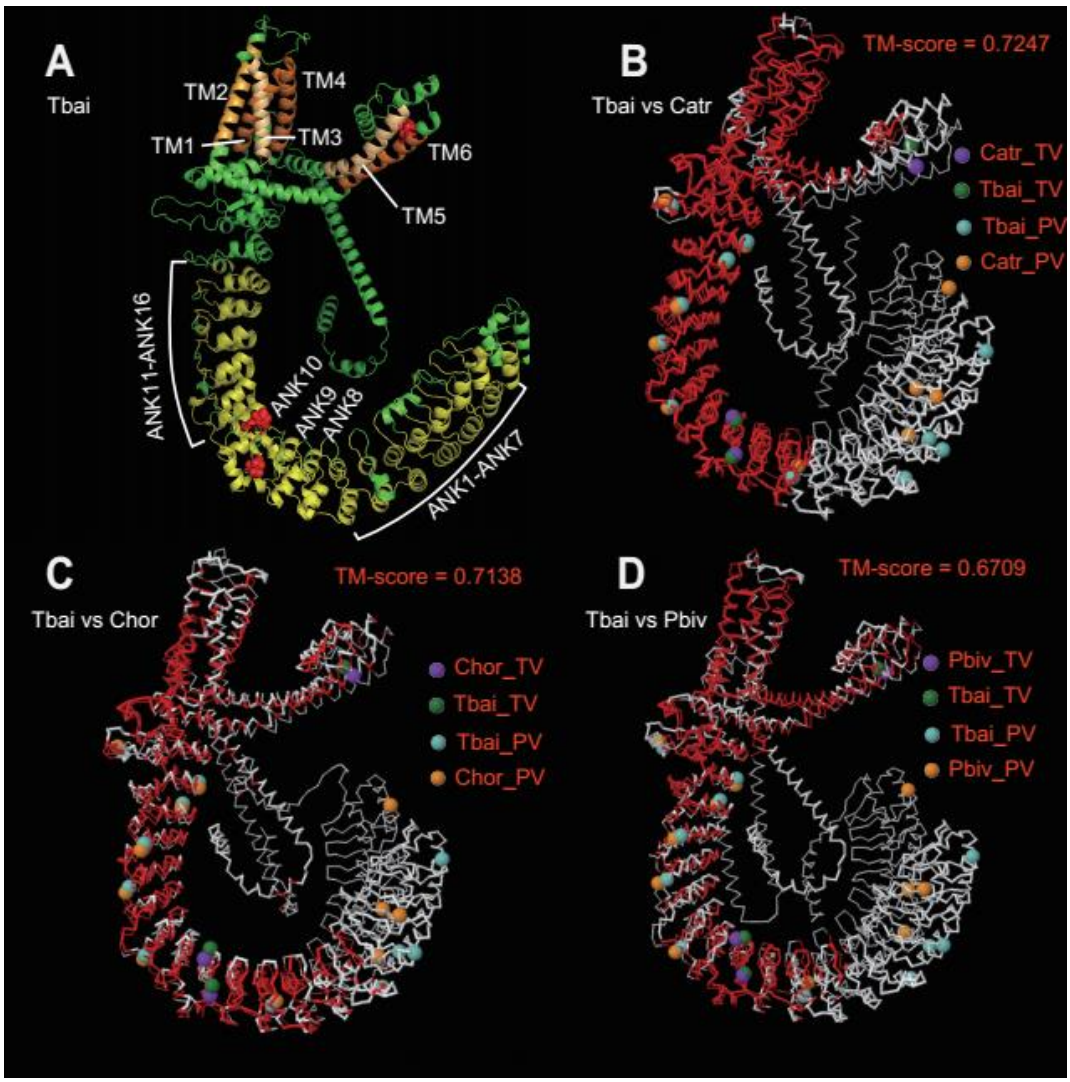

Figure S8. 3D structural modification of TRPA1 associated with *T. baileyi* specific and infrared imaging snake specific variations. (A**)** 3D structure of *T. baileyi* TRPA1 predicted by Alphafold2, the 16 ANK domains were in yellow, and the 6 TM domains were in orange and light orange, the names of the domains were marked around functional domains. **(**B) superposition of TRPA1 between *T. baileyi* (in thick wireframes) and *Crotalus atrox* (Catr) (in thin wireframes). (C) superposition of TRPA1 between *T. baileyi* (in thick wireframes) and *Corallus hortulanus* (Chor) (in thin wireframes). (D) superposition of TRPA1 between *T. baileyi* (in thick wireframes) and *python bivittatus* (Pbiv) (in thin wireframes). The TM-score of these superpositions were depicted on the left top, and residues with d<5Å were in red, and the amino acid loci of *T. baileyi* specific amino acid variation (with tag "_TV") sites and Pit-bearing specific variation (with tag "_PV") sites were marked with green/purple and light-blue/orange circles, respectively.

Supplementary Tables:

Table S1. The distribution information of hot-springs that found hot-spring snakes.

SID	Lon_S	Lat_S	Elev_S	Thermal Spring	Lon_T	Lat_T	Elev_T	Temp (℃)
S1	86.61667	29.13333	4,412	Tt26	86.61111	29.16806	4,400	23
S2	87.45	29.40694	4,446	Th25	87.45	29.40694	4,480	75
S3	87.565	28.91	4,641	Th30	87.565	28.91	4,600	45
S4	87.74026	29.0734	4,016	Th31	87.74028	29.07361	3,995	50
S5	88.17085	28.82688	4,621	Th26	87.42778	29.09028	4,200	76
S6	89.25163	30.13595	4,562	Geda	89.25163	30.13595	4,562	30
S7	89.38486	29.90155	4,336	Th45	89.38889	29.9	4,500	82
S8	89.63333	29.71111	4,702	Tb31	89.63333	29.71111	4,450	> 84
S9	90.05	29.10972	4,136	Th53	90.05	29.10972	4,000	60
S10	90.28782	29.84806	4,609	Tb33	90.37139	29.73472	4,600	90
S11	90.35222	29.98056	4,413	Th58	90.35222	29.98056	4,400	78
S12	90.59306	30.2	4,617	Th57	90.59306	30.2	4,480	46.5
S13	90.9432	30.41333	4,250	Tb36	90.94444	30.41278	4,250	> 87
S14	91.23394	30.62081	4,549	Th55	91.23333	30.61861	4,630	67
S15	92.16667	30.15278	4,441	Th64	92.16667	30.15278	4,350	46
S16	92.24091	29.69332	4,379	Tw24	92.26111	29.68611	4,380	36
S17	92.31536	29.38176	3,909	Th123	92.31528	29.3875	3,920	50.5
S18	92.49961	29.89313	4,209	Tw56	92.48806	29.89583	4,200	43
S19	93.1755	30.20246	3,962	Sangla	93.1755	30.20246	3,962	30
S20	93.34408	29.73553	3,683	Tw57	93.34444	29.73417	3,660	43

Note: SID: sample ID of *T. baileyi*; Lon_S: longitude of sample Lat_S: latitude of sample; Elev_S: elevation of sample; Lon_T: longitude of thermal spring site; Lat_T: latitude of thermal spring site; Elev_T: elevation of thermal spring site; Temp: temperature of thermal spring site. The distribution of hot-springs was collected from published records (see the Method section). The hot-spring snake's distribution information was collected from the collection of specimens (Herpetological Museum, Chengdu Institute of Biology, Chinese Academy of Sciences, Chengdu, China) and combined with the published information (see the Method section).

Table.S2 Geographic information of *T. baileyi* collected in specimen and relative literatures.

Sample ID	longitude	latitude	attitude	Source
GBJDsx_1	93.34	29.74	3,709	Specimens
GBJDlp_9	93.18	30.2	3,961	Specimens
MZGKrd_11	92.28	29.69	4,450	Specimens
MZGKmb_17	92.14	30.15	4,531	Specimens
MZGKmb_18	92.14	30.15	4,531	Specimens
SRWK_21	92.29	29.36	3,893	Specimens
YBJjd_24	90.35	29.98	4,417	Specimens
YBJjd_25	90.35	29.98	4,417	Specimens
YBJjd_26	90.35	29.98	4,417	Specimens
DXgd_30	90.29	29.85	4,578	Specimens
DXgd_31	90.29	29.85	4,578	Specimens
DXgd_32	90.29	29.85	4,578	Specimens
DXgt_34	91.23	30.62	4,549	Specimens
DXgt_35	91.23	30.62	4,549	Specimens
DXgt_36	91.23	30.62	4,549	Specimens
YBJld_41	90.65	30.16	4,853	Specimens
RBCB_42	90.06	29.11	4,116	Specimens
NMLL_44	89.38	29.9	4,365	Specimens
SJ_49	88.17	28.83	4,609	Specimens
SJ2_56	88.14	28.84	4,536	Specimens
NMLR_57	89.24	30.13	4,629	Specimens
GBJDlp_8	93.18	30.2	3,961	Specimens
GBJDlp_10	93.18	30.2	3,961	Specimens
MZGKrd_12	92.28	29.69	4,450	Specimens
SRWK_22	92.29	29.36	3,893	Specimens
SRWK_23	92.29	29.36	3,893	Specimens
YBJjd_27	90.35	29.98	4,417	Specimens
YBJjd_28	90.35	29.98	4,417	Specimens
YBJjd_29	90.35	29.98	4,417	Specimens
DXgd_33	90.29	29.85	4,578	Specimens
NMX	90.22	29.41	3,790	Specimens
H25	29.1	86.6	4,323	Hofmann et al., 2014
H26	29.4	87.4	4,155	Hofmann et al., 2014
H27	28.9	87.6	4,596	Hofmann et al., 2014
H28	29.1	87.7	4,013	Hofmann et al., 2014
H29	28.8	88.2	4,602	Hofmann et al., 2014
H30	29.9	89.1	4,256	Hofmann et al., 2014
H31	29.9	89.4	4,372	Hofmann et al., 2014
H32	29.7	89.6	4,386	Hofmann et al., 2014
H33	29.1	90.1	4,087	Hofmann et al., 2014

H34	29.9	90.4	4,395	Hofmann et al., 2014
H35	30	90.4	4,395	Hofmann et al., 2014
H36	30.2	90.7	4,887	Hofmann et al., 2014
H37	30.4	90.9	4,210	Hofmann et al., 2014
H38	30.6	91.2	4,333	Hofmann et al., 2014
H39	30.2	92.2	4,425	Hofmann et al., 2014
H40	29.7	92.2	4,382	Hofmann et al., 2014
H41	29.4	92.3	3,904	Hofmann et al., 2014
H42	29.9	92.5	4,167	Hofmann et al., 2014
H43	30.2	93.2	3,928	Hofmann et al., 2014
H44	29.7	93.3	3,652	Hofmann et al., 2014
H45	30.06	90.49	4,100	Huang et al., 2009

Notes: All the hot-spring snake specimens information were collected from the Herpet ological Museum, Chengdu Institute of Biology, Chinese Academy of Sciences, Cheng du, China.

Table S3. Sequencing Data for *T. baileyi* genome *de novo* assembly.

platform	Category	Information
PacBio	Subreads reads	15,319,559
	Subreads base	204,159,818,114
	Average subreads length	13,326.74
	Max Subreads length	145,876
	Accuracy	0.8000
	Subreads n50	21,712
	GC mean	0.4300
Hi-C Illumina	Read Length (bp)	50
	Raw Paired-end Reads	669,432,650
	Raw Bases (bp)	200,829,795,000
	Clean Paired-end Reads	658,916,714
	Clean Paired-end Reads Rate (%)	98.43
	Low-quality Paired-end Reads	4,259,028
	Low-quality Paired-end Reads Rate (%)	0.64
	Ns Paired-end Reads	119
	Ns Paired-end Reads Rate (%)	0.0
	Adapter Polluted Paired-end Reads	6,256,789
	Adapter Polluted Paired-end Reads Rate (%)	0.93
	Raw Q30 Bases Rate (%)	90.45
	Clean Q30 Bases Rate (%)	93.66

Notes: the Illumina pair-end data from our previous study was used.[6]

Table S4. Quality metrics for *T. baileyi* genome compared to other published snake genomes.

species	Size (Gb)	Scaffold N50 (bp)	Contig N50 (bp)	BUSCO
Thermophis baileyi	**1.85**	**139,893,437**	**4,023,894**	**97.10%**
Thermophis baileyi (previous version)	1.74	2,413,955	16,800	97.0%
Boa constrictor	1.45	16,597,778	47,284	94.10%
Python bivittatus	1.44	213,970	10,658	88.50%
Notechis scutatus	1.67	5,997,050	31,763	86.60%
Ophiophagus Hannah	1.59	241,519	5,201	85.50%
Pseudonaja textilis	1.59	14,685,528	50,443	87.40%
Crotalus viridis	1.34	139,167	15,735	83.30%
Naja naja	1.77	224,088,900	302,474	89.50%
Hydrophis curtus	1.62	1,346,643	183,470	91.10%
Deinagkistrodon acutus	1.47	2,122,253	22,424	-
Protobothrops flavoviridis	1.41	467,050	3,798	92.7%

Notes: the previous version of assembly is from our previous study.[6]

Table S5. Comparation of gene structure and function annotation between previous and update *T. baileyi* genome.

	Tbai_pre	Tbai_chr	*P*-value of t.test
Average length of exons	213.4788	224.2122	< 2.2e-16
Average length of introns	2,769.333	3,851.796	< 2.2e-16
Average length of genes	24,496.51	32,007.81	< 2.2e-16
number of exons	191,915	195,679	
number of genes	20,995	22,242	
number of introns	170,920	173,437	
Annotated in Swissprot	18,978	19,277	
Annotated in NR(NCBI)	19,832	20,323	

Notes: Average length of exons, introns and genes were significantly longer than in the previous genome edition. The total number of structure annotated genes, as well as functionally annotated genes in the public database is increased.

Table S6. GO enrichment of EBR related genes.

GO ID	Term names	*P*-adjust
GO:0045095	keratin filament	4.51E-13
GO:0002474	antigen processing and presentation of peptide antigen via MHC class I	9.17E-08
GO:0032611	interleukin-1 beta production	9.17E-08
GO:0032620	interleukin-17 production	1.88E-07
GO:0042612	MHC class I protein complex	2.04E-07
GO:0002367	cytokine production involved in immune response	2.04E-07
GO:0031424	keratinization	2.35E-05
GO:0050829	defense response to Gram-negative bacterium	3.08E-05
GO:0005882	intermediate filament	0.000974
GO:0070268	cornification	0.002089
GO:1901585	regulation of acid-sensing ion channel activity	0.004131
GO:0004745	retinol dehydrogenase activity	0.004355
GO:0003677	DNA binding	0.004355
GO:0098793	presynapse	0.019258
GO:0044829	positive regulation by host of viral genome replication	0.029051
GO:0005783	endoplasmic reticulum	0.037057
GO:0034338	short-chain carboxylesterase activity	0.038794
GO:0009056	catabolic process	0.038794
GO:0070895	negative regulation of transposon integration	0.038794

Table S7. Evolutionary changes in high altitude adaptation related genes.

(Excel Table)

Table S8. GO enrichment of common rapidly evolving genes among high-altitude species.

(Excel Table)

Table S9. KEGG enrichment of common rapidly evolving genes among high-altitude species.

KEGG name	ID	*p*-adjust
Metabolic pathways	k01100	3.30E-12
MAPK signaling pathway	k04010	7.30E-10
PI3K-Akt signaling pathway	k04151	1.56E-06
Pathways in cancer	k05200	5.91E-06
Rap1 signaling pathway	k04015	1.72E-05
Focal adhesion	k04510	2.39E-05
Transcriptional misregulation in cancer	k05202	9.17E-05
Regulation of actin cytoskeleton	k04810	0.000189308
EGFR tyrosine kinase inhibitor resistance	k01521	0.000771625
Ras signaling pathway	k04014	0.001186636
Hepatitis B	k05161	0.001293284
AGE-RAGE signaling pathway in diabetic complications	k04933	0.001361115
Phospholipase D signaling pathway	k04072	0.001442728
Protein processing in endoplasmic reticulum	k04141	0.00145693
Proteoglycans in cancer	k05205	0.00168059
Yersinia infection	k05135	0.002005367
Cholesterol metabolism	k04979	0.002078751
Prostate cancer	k05215	0.003358321
Epstein-Barr virus infection	k05169	0.003713852
FoxO signaling pathway	k04068	0.004000239
NF-kappa B signaling pathway	k04064	0.004098434
Neurotrophin signaling pathway	k04722	0.005084722
T cell receptor signaling pathway	k04660	0.005127997
Lysine degradation	k00310	0.005268852
Inositol phosphate metabolism	k00562	0.005576324
Parathyroid hormone synthesis, secretion and action	k04928	0.006049873
Glycerolipid metabolism	k00561	0.006124127
Th17 cell differentiation	k04659	0.0062812
NOD-like receptor signaling pathway	k04621	0.006720263
Small cell lung cancer	k05222	0.007100647
Fc gamma R-mediated phagocytosis	k04666	0.007446968
Toxoplasmosis	k05145	0.008797727
Acute myeloid leukemia	k05221	0.008797727
Glycerophospholipid metabolism	k00564	0.008797727
Choline metabolism in cancer	k05231	0.009786539
Phosphatidylinositol signaling system	k04070	0.009786539
Human papillomavirus infection	k05165	0.010126579
Tight junction	k04530	0.010126579

Epithelial cell signaling in Helicobacter pylori infection	k05120	0.011351488
Porphyrin and chlorophyll metabolism	k00860	0.011351488
Colorectal cancer	k05210	0.011351488
Gap junction	k04540	0.012989967
Longevity regulating pathway	k04211	0.013602879
Cellular senescence	k04218	0.014009151
Human T-cell leukemia virus 1 infection	k05166	0.014470883
Gastric acid secretion	k04971	0.015060862
GnRH signaling pathway	k04912	0.016832549
Gastric cancer	k05226	0.019148968
Oxytocin signaling pathway	k04921	0.022273769
Glycosylphosphatidylinositol (GPI)-anchor biosynthesis	k00563	0.024412668
Insulin signaling pathway	k04910	0.025215354
ErbB signaling pathway	k04012	0.02691036
Chagas disease (American trypanosomiasis)	k05142	0.027576351
ECM-receptor interaction	k04512	0.028173193
Fanconi anemia pathway	k03460	0.028258152
C-type lectin receptor signaling pathway	k04625	0.028628054
Human cytomegalovirus infection	k05163	0.030484598
Hypertrophic cardiomyopathy (HCM)	k05410	0.031808325
Fatty acid metabolism	k01212	0.031923485
HIF-1 signaling pathway	k04066	0.033057447
Thermogenesis	k04714	0.035618116
Non-alcoholic fatty liver disease (NAFLD)	k04932	0.035618116
Chronic myeloid leukemia	k05220	0.035912229
Leukocyte transendothelial migration	k04670	0.03664993
MicroRNAs in cancer	k05206	0.036887623
Basal transcription factors	k03022	0.037959413
Vascular smooth muscle contraction	k04270	0.037959413
Antifolate resistance	k01523	0.038208686
Calcium signaling pathway	k04020	0.038617048
mTOR signaling pathway	k04150	0.039618232
Endocrine resistance	k01522	0.04236655
Apoptosis	k04210	0.04236655
Notch signaling pathway	k04330	0.044712698
Tuberculosis	k05152	0.046289201
Inflammatory mediator regulation of TRP channels	k04750	0.046290161
Malaria	k05144	0.047548687

Table S10. GO enrichment of expanded gene families in *T. baileyi*.

(Excel Table)

Table S11. Evolutionary changes in hot-spring snake TRP genes.

Gene ID	Gene name	EBR	CNE	UNIQ	PSG	REG	Species-specific replacements	Common rapidly evolving genes
Tbai_Scaffold30_G00069	TRPA1	0	0	1	0	0	1	0
Tbai_Scaffold43_G00023	TRPC1	0	0	0	0	0	0	1
Tbai_Scaffold149_G00019	TRPC4AP	0	0	0	1	1	0	1
Tbai_Scaffold306_G00001	TRPC5	1	0	0	0	0	0	0
Tbai_Scaffold196_G00018	TRPC6	0	0	0	0	0	0	1
Tbai_Scaffold485_G00003	TRPC7	0	0	1	0	1	0	0
Tbai_Scaffold151_G00038	TRPM1	0	0	0	0	1	0	0
Tbai_Scaffold42_G00048	TRPM5	0	0	1	0	0	0	1
Tbai_Scaffold37_G00094	TRPM7	0	1	1	0	0	0	0
Tbai_Scaffold571_G00004	TRPM8	0	0	0	0	0	0	1
Tbai_Scaffold312_G00014	TRPV3	0	0	0	0	1	0	0
Tbai_Scaffold115_G00029	TRPV4	0	0	0	0	0	1	0

EBR: Evolutionary break region related genes; CNE: Conserved non-coding element related genes; UNIQ: *T. baileyi*-specific genome region related genes; PSG: Positively selected genes; REG: Rapidly evolving genes.

Table S12. Functional prediction of TRPA1 and TRPV4 genes using PROVEAN

genes	substitution	PROVEAN score	Prediction (cutoff = -2.5)
TRPA1	L376V	-0.258	Neutral
TRPA1	L380H	-3.317	Deleterious
TRPA1	L941F	-3.19	Deleterious
TRPV4	T500K	-0.291	Neutral

Notes: the cutoff score is -2.5. When the PROVEAN score is larger than -2.5, it is classified as neutral; when the PROVEAN score is smaller than -2.5, it is classified as deleterious.

Table S13. GO enrichment of hot-spring snake unique genes

(Excel Table)

Table S14. GO enrichments of CNE related genes

GO ID	Term name	p-adjusted
GO:0009952	anterior/posterior pattern specification	1.59E-08
GO:0048704	embryonic skeletal system morphogenesis	0.00461
GO:0000981	DNA-binding transcription factor activity, RNA polymerase II-specific	0.00718
GO:0007416	synapse assembly	0.02015
GO:0000122	negative regulation of transcription by RNA polymerase II	0.02035
GO:0007399	nervous system development	0.02452
GO:0000790	nuclear chromatin	0.02751
GO:0050953	sensory perception of light stimulus	0.02751
GO:0030426	growth cone	0.02751
GO:0033674	positive regulation of kinase activity	0.02751
GO:0010842	retina layer formation	0.02751
GO:0048666	neuron development	0.02751
GO:0035116	embryonic hindlimb morphogenesis	0.02751
GO:0046974	histone methyltransferase activity (H3-K9 specific)	0.02751
GO:0001228	DNA-binding transcription activator activity, RNA polymerase II-specific	0.02751
GO:0006468	protein phosphorylation	0.02807
GO:0016604	nuclear body	0.02807
GO:0007156	homophilic cell adhesion via plasma membrane adhesion molecules	0.03431
GO:0098684	photoreceptor ribbon synapse	0.03431
GO:0000978	RNA polymerase II cis-regulatory region sequence-specific DNA binding	0.03431
GO:0005001	transmembrane receptor protein tyrosine phosphatase activity	0.04844

Table S15. Genome data used in this study.

Deposited data	Abbreviation	Source	Accession NO./website
Thermophis baileyi	Tbai	This Paper	https://ngdc.cncb.ac.cn, PRJCA007342
Pseudonaja textilis	Ptex	NCBI	GCA_900608585.1
Pantherophis guttatus	Pgut	NCBI	GCF_001185365.1
Protobothrops mucrosquamatus	Pmuc	NCBI	GCF_001527695.2
Ophiophagus hannah	Ohan	NCBI	GCA_000516915.1
Python bivittatus	Pbiv	NCBI	GCF_000186305.1
Thamnophis sirtalis	Tsir	NCBI	GCF_001077635.1
Crotalus viridis viridis	Cvir	NCBI	GCA_003400415.2
Notechis scutatus	Nscu	NCBI	GCF_900518725.1
Deinagkistrodon acutus	Dacu	GigaBase	ftp.cngb.org/pub/gigadb/pub/10.5524/100001_101000/100196/
Thamnophis elegans	Tele	NCBI	GCF_009769535.1
Naja naja	Nnaj	NCBI	GCA_009733165.1
Boa constrictor	Bcon	figshare	https://doi.org/10.6084/m9.figshare.9793013.v2
Hydrophis curtus	Hcur	figshare	https://doi.org/10.6084/m9.figshare.11391606.v5
Lacerta agilis	Lagi	NCBI	GCF_009819535.1
Podarcis muralis	Pmur	NCBI	GCF_004329235.1
Zootoca vivipara	Zviv	NCBI	GCF_011800845.1
Salvator merianae	Smer	NCBI	GCA_003586115.2
Varanus komodoensis	Vkom	NCBI	GCF_004798865.1
Chrysemys picta bellii	Cpic	Ensembl	ftp.ensembl.org:/pub/release-102/fasta/chrysemys_picta_bellii
Pelodiscus sinensis	Psin	Ensembl	ftp.ensembl.org:/pub/release-102/fasta/pelodiscus_sinensis
Chelonia mydas	Cmyd	NCBI	GCF_015237465.1
Alligator mississippiensis	Amis	NCBI	GCF_000281125.3
Crocodylus porosus	Cpor	Ensembl	ftp.ensembl.org:/pub/release-102/fasta/crocodylus_porosus
Alligator sinensis	Asin	NCBI	GCF_000455745.1
Latimeria chalumnae	Lcha	Ensembl	ftp.ensembl.org:/pub/release-102/fasta/latimeria_chalumnae
Nanorana parkeri	Npar	NCBI	GCF_000935625.1
Xenopus tropicalis	Xtro	Ensembl	ftp.ensembl.org:/pub/release-102/fasta/xenopus_tropicalis
Leptobrachium leishanense	Llei	NCBI	GCA_009667805.1
Mus musculus	Mmus	Ensembl	ftp.ensembl.org:/pub/release-102/fasta/mus_musculus
Homo sapiens	Hsap	Ensembl	ftp.ensembl.org:/pub/release-102/fasta/homo_sapiens

Gallus gallus	Ggal	Ensembl	ftp.ensembl.org:/pub/release-102/fasta/gallus_gallus
Anas platyrhynchos	Apla	Ensembl	ftp.ensembl.org:/pub/release-102/fasta/anas_platyrhynchos
Parus humilis	Phum	NCBI	GCF_000331425.1
Bos grunniens	Bmut	NCBI	GCF_000298355.1
Ochotona curzoniae	Ocur	NCBI	GCF_017591425.1
Equus caballus	Ecab	NCBI	GCF_002863925.1
Falco naumanni	Fnau	NCBI	GCF_017639655.2
Ornithorhynchus anatinus	Oana	NCBI	GCF_004115215.2
Parus major	Pmaj	NCBI	GCF_001522545.3
Taeniopygia guttata	Tgut	NCBI	GCF_003957565.2

Supplementary videos:

The behavioral experiments on the thermotropic behavior of three species of snakes (*T. baileyi*, *Pantherophis guttatus*, *Pareas menglaensis*). The Video demos showed their choices when faced with cold stimuli.